

RICE UNIVERSITY

**Full-duplex Wireless: Design, Implementation and  
Characterization.**

by

**Melissa Duarte**

A THESIS SUBMITTED  
IN PARTIAL FULFILLMENT OF THE  
REQUIREMENTS FOR THE DEGREE

**Doctor of Philosophy**

APPROVED, THESIS COMMITTEE:

---

Ashutosh Sabharwal *Chair*  
Associate Professor of Electrical and  
Computer Engineering

---

Behnaam Aazhang  
J. S. Abercrombie Professor of Electrical and  
Computer Engineering

---

Richard Tapia  
University Professor and Maxfield-Oshman Professor  
of Computational and Applied Mathematics

---

Lin Zhong  
Associate Professor of Electrical and Computer  
Engineering

---

Chris Dick  
Distinguished Engineer and DSP Chief Architect  
at Xilinx

HOUSTON, TEXAS

APRIL 2012

## ABSTRACT

# **Full-duplex Wireless: Design, Implementation and Characterization.**

by

**Melissa Duarte**

One of the fundamental assumptions made in the design of wireless networks is that the wireless devices have to be half-duplex, i.e., they cannot simultaneously transmit and receive in the same frequency band. The key deterrent in implementing a full-duplex wireless device, which can simultaneously transmit and receive in the same frequency band, is the large power differential between the self-interference from a device's own transmissions and the signal of interest coming from a distant source. In this thesis, we revisit this basic assumption and propose a full-duplex radio design. The design suppresses the self-interference signal by employing a combination of passive suppression, and active analog and digital cancellation mechanisms. The active cancellations are designed for wideband, multiple subcarrier (OFDM), and multiple antenna (MIMO) wireless communications systems. We then implement our design as a 20 MHz MIMO OFDM system with a 2.4 GHz center frequency, suitable for Wi-Fi systems. We perform extensive over-the-air tests to characterize our implementation. Our main contributions are the following: (a) the average amount of active cancellation increases as the received self-interference power increases and as a result, the rate of a full-duplex link increases as the transmit power of communicating devices increases, (b) applying digital cancellation after analog cancellation can sometimes increase the self-interference and the effectiveness of digital cancellation in a full-duplex system will depend on the performance of the cancellation stages

that precede it, (c) our full-duplex device design achieves an average of 85 dB of self-interference cancellation over a 20 MHz bandwidth at 2.4 GHz, which is the best cancellation performance reported to date, (d) our full-duplex device design achieves 30–84% higher ergodic rates than its half-duplex counterpart for received powers in the range of  $[-75, -60]$  dBm. As a result, our design is the first one to achieve Wi-Fi ranges; in comparison, no implementation to date has achieved Wi-Fi ranges. Consequently, we have conclusively demonstrated that Wi-Fi full-duplex is practically feasible and hence shown that one of the commonly made assumptions in wireless networks is not fundamental.

# Table of Contents

|          |   |           |
|----------|---|-----------|
| <b>1</b> | <b>Introduction</b>   | <b>1</b>  |
| 1.1      | Main Challenge in Full-duplex Wireless Communications . . . . . | 1         |
| 1.2      | Opportunity and Impact of Practical Full-duplex . . . . .       | 2         |
| 1.3      | Key Innovations In This Thesis . . . . .                        | 3         |
| 1.3.1    | Per-subcarrier Self-interference Cancellation . . . . .         | 4         |
| 1.3.2    | Self-interference Cancellation for Multiple Antennas . . . . .  | 5         |
| 1.4      | Key Results . . . . .   | 7         |
| 1.4.1    | Range Extension . . . . .                                       | 7         |
| 1.4.2    | Performance of Active Cancellation . . . . .                    | 7         |
| 1.4.3    | Total Achieved Cancellation . . . . .                           | 8         |
| 1.5      | Outline of the Thesis . . . . .                                 | 9         |
| <b>2</b> | <b>Full-Duplex Device Design</b>                                | <b>10</b> |
| 2.1      | Passive Suppression . . . . .                                   | 10        |
| 2.2      | Active Analog Cancellation . . . . .                            | 12        |
| 2.3      | Active Digital Cancellation . . . . .                           | 15        |
| <b>3</b> | <b>Experiment setup and Implementation</b>                      | <b>16</b> |
| 3.1      | Node Locations . . . . .  | 16        |
| 3.2      | Full-duplex and Half-duplex Systems Considered . . . . .        | 16        |

| Chapter   | Page      |
|---|-----------|
| 3.3 WARPLab Implementation . . . . .  | 19        |
| 3.4 Power and Self-Interference Cancellation Measurements for System<br>Characterization . . . . .          | 20        |
| 3.4.1 Transmitter Power . . . . .   | 21        |
| 3.4.2 Received Signal of Interest Power . . . . .   | 22        |
| 3.4.3 Received Self-Interference Power . . . . .  | 22        |
| 3.4.4 Self-Interference Power after Passive and Analog Cancellation   | 22        |
| 3.4.5 Self-Interference Power after Passive, Analog, and Digital Can-<br>cellation . . . . .                | 23        |
| 3.4.6 Amount of Cancellation . . . . .  | 23        |
| 3.4.7 Block Diagram Showing a Subset of Power Measurements for a<br>Full-duplex $2 \times 1$ Node . . . . . | 24        |
| 3.5 Time Diagram of a Packet . . . . .  | 24        |
| 3.5.1 Time Diagram for a Full-duplex $2 \times 1$ Packet . . . . .  | 25        |
| 3.5.2 Time Diagram for a Half-duplex $3 \times 1$ Packet . . . . .  | 32        |
| <b>4 Characterization of the Self-interference Cancellation</b>   | <b>36</b> |
| 4.1 Passive Suppression . . . . .   | 36        |
| 4.2 Active Analog and Digital Cancellation . . . . .  | 37        |
| 4.3 Total Cancellation . . . . .  | 42        |
| <b>5 Full-duplex Ergodic Rates and Comparison with Half-duplex</b>  | <b>44</b> |
| 5.1 Performance Metric: Empirical Ergodic Rates . . . . .   | 44        |
| 5.2 Full-duplex Ergodic Rates with Increasing Power . . . . .   | 45        |
| 5.3 Comparison of Full-duplex and Half-duplex Systems . . . . .   | 49        |

| Chapter  | Page      |
|--|-----------|
| 5.3.1 Power Assignment for Fair Comparison between Full-duplex<br>and Half-duplex . . . . .  | 49        |
| 5.3.2 Comparison of Full-duplex and Half-duplex Ergodic Rates . .                            | 51        |
| 5.4 Importance of Per-Subcarrier Cancellation . . . . .                                      | 54        |
| 5.4.1 Analysis of the Cancellation Coefficient Required Per Subcarrier                       | 55        |
| 5.4.2 Effects of Analog Cancellation and Frequency Selectivity on<br>Ergodic Rates . . . . . | 57        |
| <b>6 Conclusion</b>  | <b>60</b> |
| 6.1 Significance and Implications . . . . .  | 60        |
| 6.2 Future Directions . . . . .  | 61        |
| <b>BIBLIOGRAPHY</b>  | <b>62</b> |

## 1.1 Main Challenge in Full-duplex Wireless Communications

Current deployed wireless communication systems employ devices which use either a time-division or frequency-division approach for wireless transmission and reception of signals. This requires dividing the temporal and/or spectral resources into orthogonal resources and results in an orthogonalization of the transmissions and receptions performed by a wireless device. Consequently, all currently deployed wireless devices operate in half-duplex fashion, where same frequency simultaneous transmission and reception of signals is not possible.

The key challenge in achieving full-duplex wireless communications, where a device can transmit and receive signals over-the-air at the same time and in the same frequency band, is the large power differential between the self-interference created by a device's own wireless transmissions and the received signal of interest coming from a distant transmitting antenna. This large power differential is due to the fact that the self-interference signal has to travel much shorter distances than the signal of interest. The large self-interference spans most of the dynamic range of the Analog to Digital Converter (ADC) in the received signal processing path, which in turn dramatically increases the quantization noise for the signal-of-interest. Thus to achieve full-duplex it is essential to suppress the self-interference *before* the analog received signal is sampled by the ADC.

Current wireless network designs have assumed that the power differential between

the self-interference and the signal of interest is such that it is impossible to cancel the self-interference enough in order to make full-duplex wireless communications feasible.

## 1.2 Opportunity and Impact of Practical Full-duplex

Cellular, Wi-Fi, Bluetooth, and Femto-cell networks are arguably the four most commonly used wireless networks. Out of these four networks, the first one to be deployed was the cellular network, which operates at distances in the order of kilometers and uses mobile devices which transmit at powers close to 30 dBm. For these values of transmit powers and distances between communicating devices, it seemed unfeasible to cancel the self-interference enough to enable full-duplex wireless communications. Consequently, the impossibility of full-duplex wireless communications remained the paradigm for wireless networks design. However, as new wireless networks like Wi-Fi, Bluetooth, and Femto-cells have been deployed, we observe a common trend: the transmission powers and the distance between communicating devices has decreased compared to cellular networks, while the size and computation power of mobile devices has either remained the same or sometimes increased (e.g. laptops). As a result, the power differential between the self-interference and the signal of interest is expected to be lower for full-duplex communications in Wi-Fi, Bluetooth, or Femto-cell networks, compared to the power differential that would be expected in a full-duplex cellular network. Furthermore, the processing power of mobile devices is such that one can think of the possibility of designing algorithms for self-interference cancellation that can be implemented using the resources available in current devices. This naturally leads to the following question: could the self-interference in Wi-Fi, Bluetooth, or Femto-cell networks be cancelled enough to enable full-duplex communications? As we will demonstrate in this thesis, the answer to this question is yes. Specifically, we will demonstrate the feasibility and advantages of full-duplex communications for

Wi-Fi-like systems.

Our demonstration of full-duplex wireless communications in practical scenarios breaks the most fundamental assumption that has been made in network design - that all practical wireless transmissions have to be half-duplex. We believe that our demonstration of practical full-duplex wireless communications will spur application and protocol innovations that could conflate the throughput benefit of full-duplex beyond the gains reported in this thesis.

### 1.3 Key Innovations In This Thesis

Full-duplex experimental demonstrations for narrowband wireless communication systems were first reported in 1998 [1]. Since then, multiple authors [2–8] have reported different methods and implementations for larger bandwidths and/or multiple transmit antennas as we will explain with more detail later in this section. However, all previously reported full-duplex implementations only achieve ranges shorter than 10 m in line-of-sight conditions, which corresponds to more than -60 dBm of received signal strength (RSSI). Hence, previously reported full-duplex implementations are not practical for most wireless standards. *Our full-duplex device design is the first one to operate at 20 MHz bandwidth using multiple subcarriers and multiple transmitter antennas, and it is the first one to achieve full-duplex gains over Wi-Fi ranges.* More specifically, our full-duplex device design results in ergodic rate gains of 30% to 84% over its half-duplex counterpart for RSSI values between  $[-75, -60]$  dBm.

We note that since propagation environments vary significantly from one location to another, range is almost never specified in actual physical distance by wireless standards. Instead, wireless standards specify expected received signal strength, RSSI, which is in the range of  $[-80, -60]$  dBm for Wi-Fi. The RSSI based description of the range can be translated into physical ranges (in meters), using models that

approximate the path loss of a signal for different propagation environments [9].

The ergodic rate gains of our full-duplex device design stem from the following two innovations: (a) per-subcarrier self-interference cancellation, and (b) self-interference cancellation for multiple antennas. By combining these two innovations we are able to achieve self-interference cancellation values of 70 to 100 dB, with an average of 85 dB. This is the highest reported cancellation in open literature to date for a scheme operating at 2.4 GHz with a bandwidth of 20 MHz. This high suppression combined with the use of transmission schemes for multiple transmitter antennas yields the full-duplex rate gains achieved by our full-duplex device design. The two innovations of our full-duplex device design are explained below.

### 1.3.1 Per-subcarrier Self-interference Cancellation

Wi-Fi systems use Orthogonal Frequency Division Multiplexing (OFDM) in order to achieve wideband communication. OFDM consists in dividing the utilized frequency band into multiple sub-bands and using a different carrier tone, or sub-carrier, for transmission in each sub-band. Hence, Wi-Fi systems utilize multiple subcarriers for wideband communication and subcarriers are chosen such that they maintain orthogonal as they propagate through the channel.

Self-interference cancellation designs have been demonstrated for multiple sub-carrier systems for 5 MHz bandwidth in [4], 10 MHz bandwidth in [5], and 20 MHz bandwidth in [3]. Implementations in [4, 5, 3] achieve no more than 73 dB of self-interference cancellation and use an analog canceller based on the QHx220 chip which is designed for operation in wideband frequency flat (frequency non-selective) channels [10, 11]. Consequently, the analog self-interference cancellers demonstrated in [4, 5, 3] can operate only in self-interference channels that have a flat-frequency response. However, our extensive measurements for 20 MHz bandwidth demonstrate

that there are many practical antenna configurations in a mobile device that result in self-interference channels which are frequency selective, hence, the wireless self-interference channel varies over time and per subcarrier. From this observation we concluded that an analog canceller that can adapt over time and per-subcarrier is a better solution for analog self-interference cancellation than designs that work only in frequency flat self-interference channels. This discovery naturally led to our analog per-subcarrier canceller which tracks the self-interference channel over time and subcarriers, and thus ensures maximal gains from analog cancellation over the whole bandwidth by adapting the analog cancellation as required as a function of time and subcarrier.

### 1.3.2 Self-interference Cancellation for Multiple Antennas

We first discuss previous efforts to implement self-interference cancellation for systems with more than one transmitter and one receiver antenna. This allows us to illustrate the state of the art before highlighting the main innovations of our proposed canceller for multiple self-interfering antennas.

In [2] the authors proposed a Multiple antenna Input and Multiple antenna Output (MIMO) extension for full-duplex, tested different MIMO beam forming and nulling techniques for improving self-interference suppression, and reported improvements for a 0.1 MHz bandwidth four transmitter and three receiver antenna ( $4 \times 3$ ) MIMO communication at 370 MHz center frequency. The distance between the communicating devices was only three meters. While the results were encouraging, the short distance achieved and requirement of many antennas to achieve the gains made practical deployment impossible.

Choi et al. [4] proposed antenna cancellation using three antennas to create a beam forming null that cancels the self-interference at the receiver antenna. Apart

from manual running that prevents real time operation, this design creates null zones in numerous locations in the far field. This is undesirable since communication with a device placed in one of these null-zones will lead to communication at near-zero rate. The antenna cancellation proposed in [4] was modified in [6] in order to avoid null zones in the far field and allow cancellation for more than three antennas per device. However, the design presented in [6] is practically challenging due to the complexity of the required antenna placement and to analog circuitry requirements which increase as a function of the number of transmit and receive antennas. More importantly, the distance between communicating devices was no more than three meters in the experiments reported in [6].

Our self-interference canceller for multiple antennas has the following two novel features. First, the amount of hardware resources required for cancellation scales linearly as a function of only the number of receiver antennas. This is considerably less than prior work [6] which requires hardware that increases as a function of both the number of transmitter and receiver antennas. Second, we address the important issue of how multiple antennas should be placed around a laptop-sized mobile device. Specifically, we evaluate possible antenna placements for a two transmitter and one receiver antenna ( $2 \times 1$ ) full-duplex device. We focus on this specific full-duplex implementation because it is a practical design, for example, up until now the most widely deployed multiple antenna Wi-Fi configuration implements a half-duplex communication with two transmitter and one receiver antenna. Using extensive experimental evaluation we find an antenna placement for  $2 \times 1$  full-duplex communication which improves the amount of self-interference cancellation while allowing the well-known rate gains of multiple antenna  $2 \times 1$  communication. We note that our antenna placement together with our active per subcarrier canceller results in a design that is highly robust to device size variations, unlike antenna placements to create beam

forming nulls [4, 6] which are very sensitive to the relative location of antennas and any material around them. Also, we note that our self-interference canceller design for multiple antennas does not impose any constraint on the design of the transmitted signals hence it allows full rank MIMO communication. In contrast, previous canceller designs for multiple antennas [4, 6] do not allow full rank multiple antenna communication.

## 1.4 Key Results

### 1.4.1 Range Extension

Our extensive experiment-based evaluation is the first one to evaluate the rate-range tradeoff of both legacy and full-duplex devices in identical scenarios, leading to the following key conclusions. First, single antenna full-duplex systems with 73 dB average cancellation perform worse than their half-duplex counterparts for RSSIs less than  $-60$  dB and are thus not suitable for Wi-Fi deployments (in-line with very short ranges achieved by prior work). Second, our  $2 \times 1$  full-duplex design has higher ergodic rate than  $2 \times 1$  half-duplex,  $3 \times 1$  half-duplex, and  $2 \times 2$  half-duplex configurations for RSSIs larger than  $-75$  dBm. This implies that the diversity benefits from multiple transmitter antennas combined with our novel self-interference cancellation design opens up the possibility of including full-duplex as a mode in Wi-Fi, where the range of operation is typically between RSSIs of  $-80$  and  $-60$  dBm.

### 1.4.2 Performance of Active Cancellation

Our experiment based characterization of active analog and active digital self-interference cancellation is the first one to demonstrate that the amount of self-interference cancellation achieved by active cancellation increases as the power of the self-interfering signal increases. This result is intuitive because the canceller relies on

estimating the self-interference channel, and a higher self-interference power implies lower channel estimation error and hence better cancellation. Related work on implementation of self-interference cancellation mechanisms [1–7] has reported measured values of the amount of active cancellation that can be achieved, but a characterization of the amount of cancellation as a function of the self-interference power has not been reported before. Our characterization of active cancellation as a function of the self-interference power allows us to show that for a constant Signal to Interference (SIR) ratio at the receiver antenna (this is the SIR before active cancellation), the rate of a full-duplex link increases as the self-interference power increases. This appears counter-intuitive at first but follows from the fact that the amount of self-interference cancellation increases with increasing self-interference power. This result leads us to a design rule for full-duplex systems which specifies that for two devices that are communicating in full-duplex mode, increasing the transmission power at both devices by the same amount increases the ergodic sum rate of the full-duplex system.

### 1.4.3 Total Achieved Cancellation

Previous work [5] has conjectured that the performance of digital cancellation is independent of the cancellation stages that precede it. Hence, previous work has assumed that if digital cancellation by itself (measured in isolation) can cancel up to 30 dB then it will also cancel 30 dB when applied after analog cancellation. We demonstrate that this conclusion is *incorrect*. Intuitively, it is clear that in an ideal scenario where analog cancellation could achieve infinite dB of cancellation then having digital cancellation after analog cancellation would be unnecessary. Specifically, we show that (a) applying digital cancellation after analog cancellation can sometimes increase the self-interference and (b) the effectiveness of digital cancellation in a full-duplex system will depend on the performance of the cancellation stages that

precede it.

## 1.5 Outline of the Thesis

The rest of the thesis is organized as follows. Chapter 2 explains our full-duplex node design and implementation. The environments and scenarios under which our full-duplex implementation was evaluated are described in Chapter 3. Description of implementation parameters, signal measurements, and system time diagrams are also presented in Chapter 3. A characterization of the amount of self-interference cancellation achieved by our full-duplex implementation is presented in Chapter 4. Chapter 5 shows the rate gains achieved by our full-duplex implementation and the effects of self-interference cancellation on the achieved rates. Conclusions are presented in Chapter 6.

We present a full-duplex device design which uses a combination of passive suppression and active cancellation techniques, where passive suppression precedes active cancellation. The cancellation techniques are explained below.

## 2.1 Passive Suppression

Passive Suppression (PS) is achieved by maximizing the attenuation of the self-interference signal due to propagation path loss over the self-interference channel, which is the channel between same node transmitter and receiver antennas. The amount of passive suppression depends on the distance between antennas, the antenna directionality, and the antenna placement on the full-duplex device.

In this thesis we evaluate possible antenna placements for a two transmitter antenna and one receiver antenna ( $2 \times 1$ ) full-duplex device. We focus on this specific full-duplex implementation because it is a practical design. For example, the most widely deployed multiple antenna Wi-Fi system corresponds to  $2 \times 1$  half-duplex communication.

For our two transmit (T1, T2) and one receive (R1) antenna placement analysis we considered two possible antenna placements. For each antenna placement we considered two cases: antennas with a device in the middle and antennas without a device in the middle. Hence, we considered a total of four different configurations which are shown in Table 2.1. These same four configurations were used for half-

duplex experiments. The transmitter and receiver antenna assignment for the half-duplex experiments will be explained later in Section 3.2 when we will describe the half-duplex implementations considered.

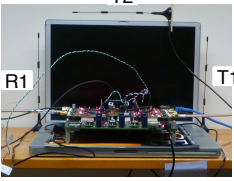
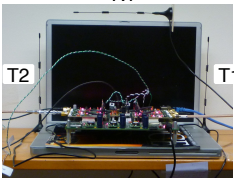
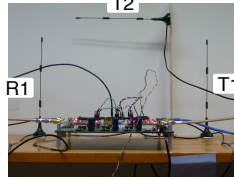
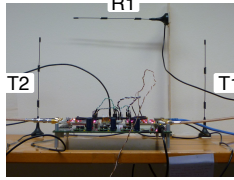
|             |           | Antenna Placement 1 (A1)  | Antenna Placement 2 (A2)   |
|-------------|-----------|---|--|
|             |           | T2 is orthogonal to T1<br>R1 is parallel to T1                                    | T2 is parallel to T1<br>R1 is orthogonal to T1                                     |
| With Device |           |  |  |
|             | No Device |  |  |

Table 2.1: Four different antenna configurations used in experiments. The distance between parallel antennas is 37.5 cm. Antenna labels correspond to antennas used for full duplex  $2 \times 1$  experiments.

The antennas used in experiments [12] are designed for 2.4 GHz operation, with vertical polarization, and have toroid-like radiation pattern shown in [12]. In Antenna Placement 1 (A1), the experiments correspond to the case where the main lobe of the receiver antenna is in the same direction as the main lobe of T1 and orthogonal to the main lobe of T2. In Antenna Placement 2 (A2), the experiments correspond to the case where the receiver main lobe is orthogonal to the main lobe of both T1 and T2. As experiments in Section 4.1 will demonstrate, the orthogonal placement of the transmitter and receiver main lobes in A2 will help reduce the self-interference. Hence A2 will result in larger passive suppression than A1. Experiment results in Section 4.1 will also demonstrate and quantify the increase in passive suppression achieved by placing antennas appropriately around a device.

We use  $\mathbf{h}_{i,m,n}$  to denote the self-interference channel between transmitter an-

tenna  $m$  and receiver antenna  $n$  at device  $i$ .  $\mathbf{h}_{i,m,n}$  varies with time and frequency. Our analysis of self-interference cancellation for multiple subcarrier (OFDM) systems will be presented in the frequency domain. We use  $h_{i,m,n}[k]$  to denote the magnitude and phase that the self-interference channel  $\mathbf{h}_{i,m,n}$  applies to subcarrier  $k$ . For a system with  $K$  subcarriers the channel vector is defined as  $\mathbf{h}_{i,m,n} = [h_{i,m,n}[1], h_{i,m,n}[2], \dots, h_{i,m,n}[K]]$ . Figure 2.1 shows the two passive cancellation paths  $\mathbf{h}_{i,1,1}$  and  $\mathbf{h}_{i,2,1}$  for a full-duplex device with two transmitter antennas and one receiver antenna. For simplicity of the drawing, the antennas in Figure 2.1 are not placed as in one of the configurations in Table 2.1.

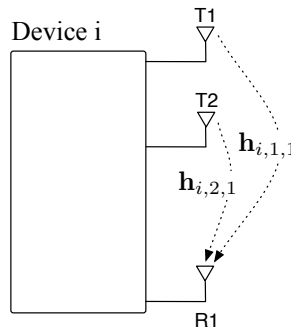


Figure 2.1: Full-duplex device with two transmitter antennas and one receiver antenna. Passive suppression consists in propagation loss through wireless self-interference channels  $\mathbf{h}_{i,1,1}$  and  $\mathbf{h}_{i,2,1}$ .

## 2.2 Active Analog Cancellation

As the name suggests, active Analog Cancellation (AC) is the active cancellation performed in analog domain *before* the received signal passes through the Analog-to-Digital Converter (ADC). For an OFDM MIMO device, the self-interference signal received at Device  $i$  antenna  $n$  on subcarrier  $k$  after passive suppression is equal to

$$y_{i,n}^{PS}[k] = \sum_{m=1}^M h_{i,m,n}[k] x_{i,m}[k] \quad (2.1)$$

where  $x_{i,m}[k]$  is the signal transmitted from Device  $i$  on subcarrier  $k$  antenna  $m$ . Analog cancellation of the self-interference at receiver antenna  $n$  is implemented by

subtracting an estimate of  $y_{i,n}^{PS}[k]$  from the received signal.

In our proposed device design, the additional hardware components required for active analog cancellation of the self-interference at one receiver antenna consist of one Digital-to-Analog converter (DAC), one transmitter radio (Tx Radio) which up converts the signal from Base Band (BB) to RF, and one RF adder. The RF adder is a passive device implemented using a power combiner [13].

Figure 2.2 shows a diagram of our proposed analog cancellation for a full-duplex OFDM device with two transmitter antennas and one receiver antenna. One input to the RF adder is the signal at the receiver antenna and the other input is a cancelling signal  $\mathbf{z}_{i,n}$  local to Device  $i$  and input to the RF adder via a wire. For subcarrier  $k$  and receiver antenna  $n$ , the local signal  $\mathbf{z}_{i,n}$  is equal to

$$z_{i,n}[k] = -h_{i,n}^W[k] \sum_{m=1}^M b_{i,m,n}[k] x_{i,m}[k] \quad (2.2)$$

where  $h_{i,n}^W[k]$  denotes the magnitude and phase that affect a signal at subcarrier  $k$  when passing through the wire connected to the RF adder at Device  $i$  receiver antenna  $n$ . Further,  $b_{i,m,n}[k]$  denotes the cancellation coefficient for the self-interference received at antenna  $n$  from transmitter antenna  $m$  at subcarrier  $k$  at Device  $i$ .

The self-interference at subcarrier  $k$  after analog cancellation at antenna  $n$  (this is the signal at the output of the RF adder connected to antenna  $n$ ) is equal to

$$y_{i,n}^{AC}[k] = y_{i,n}^{PS}[k] - z_{i,n}[k], \quad (2.3)$$

which can be rewritten as

$$y_{i,n}^{AC}[k] = \sum_{m=1}^M (h_{i,m,n}[k] - h_{i,n}^W[k] b_{i,m,n}[k]) x_{i,m}[k]. \quad (2.4)$$

From the equation for  $y_{i,n}^{AC}[k]$ , we observe that active analog cancellation achieves perfect cancellation when  $b_{i,m,n}[k] = h_{i,m,n}[k]/h_{i,n}^W[k]$ . In a real system,  $h_{i,m,n}[k]$  and

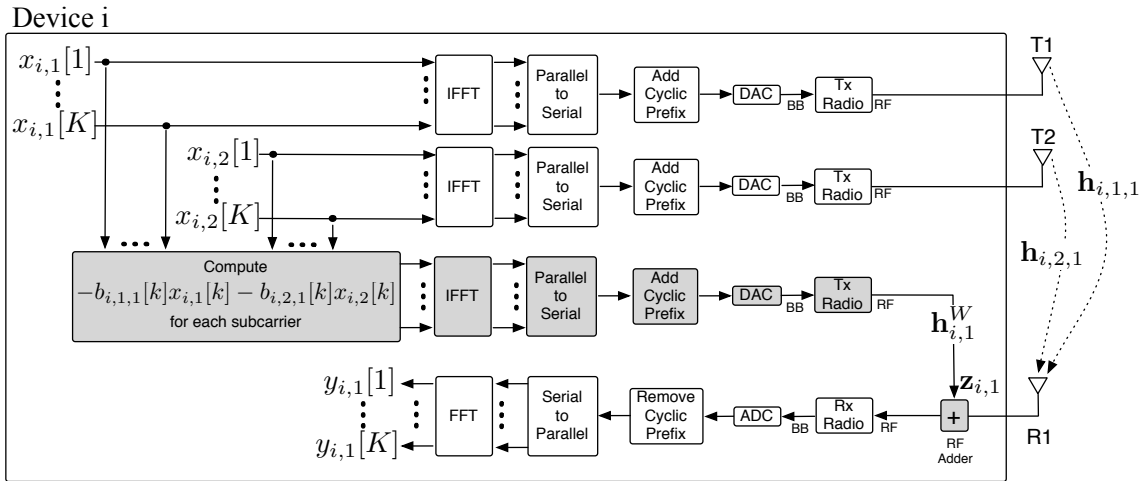


Figure 2.2: Block diagram of a full-duplex OFDM device with two transmitter antennas and one receiver antenna using passive suppression and analog self-interference cancellation. Blocks used for active analog cancellation are highlighted in gray. Passive suppression consists in propagation loss through wireless self-interference channels  $\mathbf{h}_{i,1,1}$  and  $\mathbf{h}_{i,2,1}$ .

$h_{i,n}^W[k]$  can only be estimated, which leads to the following practical computation

$$b_{i,m,n}[k] = \frac{\hat{h}_{i,m,n}[k]}{\hat{h}_{i,n}^W[k]}, \quad (2.5)$$

where  $\hat{h}_{i,m,n}[k]$  and  $\hat{h}_{i,n}^W[k]$  are the estimates of  $h_{i,m,n}[k]$  and  $h_{i,n}^W[k]$  respectively. Thus, cancellation is usually not perfect. The estimates of  $h_{i,m,n}[k]$  and  $h_{i,n}^W[k]$  are computed based on pilots sent from each transmitter radio on orthogonal time slots. Since  $h_{i,n}^W[k]$  is a wire it is a static channel and it doesn't need to be estimated often. Current Wi-Fi implementations always send pilots at the beginning of a packet, these pilots can be used for estimation of the self-interference channel  $h_{i,m,n}[k]$ , hence, estimation of the self-interference channels will not require a modification of the pilots in a packet. A time diagram of pilot and payload transmissions for a full-duplex  $2 \times 1$  packet in our specific implementation will be shown in Section 3.5.1.

It is important to notice that the additional hardware requirements of our proposed analog canceller scale only with the number of receiver antennas (linearly).

Also, any additional transmitter radio used for analog cancellation does not require a power amplifier since it is transmitting over a wire. Another important aspect to notice is that our analog cancellation does not impose any constraint on the design of transmitted signals  $x_{i,m}[k]$ .

### 2.3 Active Digital Cancellation

There is a residual self-interference  $y_{i,n}^{AC}[k]$  that remains after analog cancellation due to imperfect analog cancellation. Active Digital Cancellation (DC) estimates  $y_{i,n}^{AC}[k]$  and subtracts this estimate from the received signal in the digital domain. The estimate of  $y_{i,n}^{AC}[k]$  is computed based on a second round of pilots sent from each transmitter antenna and received while applying analog cancellation to each receiver antenna. Specifically, the second round of pilots is used to compute  $h_{i,m,n}[k] - h_{i,n}^W[k]b_{i,m,n}[k]$  which is the equivalent self interference channel after passive suppression and analog cancellation. Alternatively, the estimate of  $y_{i,n}^{AC}[k]$  can be computed without extra pilots if implemented based on correlation between the transmitted and received self-interference payload signal.

## Experiment setup and Implementation

---

### 3.1 Node Locations

Experiments were conducted inside an office building. We used five devices which we label as nodes Na, Nb, Nc, Nd, and Ne. The nodes were placed at locations shown in Figure 3.1. The five-node setup allowed us to evaluate ten different two-node links. The ten link pairs, their inter-node distance and the type of channel for each link are shown in Table 3.1. Our choices allowed us to create line-of-sight channels and also extremely challenging multi-wall propagation environments. Experiments were performed both at night and during office work hours with people walking in and out of the rooms, which represented a typical Wi-Fi deployment.

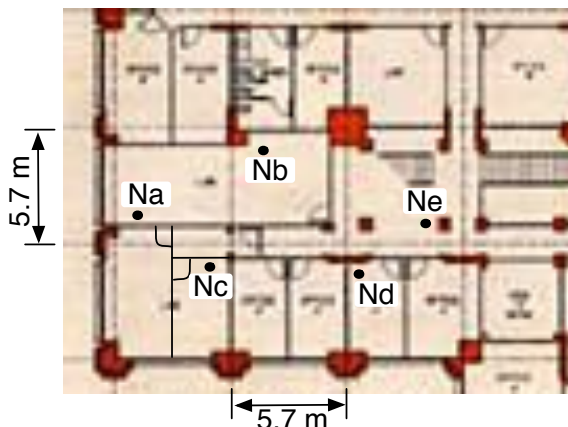


Figure 3.1: Setup locations of nodes.

### 3.2 Full-duplex and Half-duplex Systems Considered

For each of the ten links, we ran experiments for a full-duplex  $1 \times 1$  system (FD  $1 \times 1$ ), a full-duplex  $2 \times 1$  system (FD  $2 \times 1$ ), a half-duplex  $2 \times 1$  system (HD  $2 \times 1$ ), a

| Link number | Node pair | Physical Distance (m) | Type of channel | Walls crossed |
|-------------|-----------|-----------------------|-----------------|---------------|
| 1           | Na, Nb    | 6.5                   | LOS             | 0             |
| 2           | Nd, Ne    | 4.4                   | NLOS            | 1             |
| 3           | Nb, Ne    | 9.3                   | NLOS            | 1             |
| 4           | Nc, Ne    | 11.3                  | NLOS            | 1             |
| 5           | Na, Ne    | 14.8                  | NLOS            | 1             |
| 6           | Nb, Nc    | 6.5                   | NLOS            | 2             |
| 7           | Nb, Nd    | 8.3                   | NLOS            | 2             |
| 8           | Na, Nc    | 4.7                   | NLOS            | 3             |
| 9           | Nc, Nd    | 8.2                   | NLOS            | 3             |
| 10          | Na, Nd    | 12.7                  | NLOS            | 3             |

Table 3.1: Links considered in experiments

half-duplex  $3 \times 1$  system (HD  $3 \times 1$ ), and a half-duplex  $2 \times 2$  system (HD  $2 \times 2$ ). Experiment results obtained for these five systems have the necessary data to evaluate the performance of our full-duplex device design and compare its performance with half-duplex systems which use the same amount of radio resources per node. Notice that a HD  $M \times N$  node needs  $M$  transmitter radios and  $N$  receiver radios (total  $M + N$  radios) while our FD  $M \times N$  node uses  $M$  transmitter radios,  $N$  receiver radios and  $N$  radios for self-interference cancellation (total  $M + 2N$  radios) per node for any  $M, N \geq 1$ .

Table 3.2 shows the number of radios and antennas per node used by each of the full-duplex and half-duplex systems considered. We will compare the performance of full-duplex and half-duplex systems which use the same number of radios per node. The performance of FD  $2 \times 1$  will be compared with the performance of HD  $3 \times 1$  and HD  $2 \times 2$  systems. The performance of FD  $1 \times 1$  will be compared with the performance of HD  $2 \times 1$ .

For full-duplex and half-duplex experiments we considered the four different configurations shown in Table 2.1. The figures in Table 2.1 only labeled the antenna use for full-duplex communication. The antenna use for both full-duplex and half-duplex

| System | Number of antennas per node | Number of transmitter radios per node | Number of receiver radios per node | Total number of radios per node |
|--------|-----------------------------|---------------------------------------|------------------------------------|---------------------------------|
| FD 2×1 | 3                           | 3                                     | 1                                  | 4                               |
| HD 3×1 | 3                           | 3                                     | 1                                  | 4                               |
| HD 2×2 | 2                           | 2                                     | 2                                  | 4                               |
| FD 1×1 | 2                           | 2                                     | 1                                  | 3                               |
| HD 2×1 | 2                           | 2                                     | 1                                  | 3                               |

Table 3.2: Number of antennas and radios per node used by the different full-duplex and half-duplex systems that were evaluated via experiments.

communication for all the four configurations considered is shown in Table 3.3. For all the systems that use only one receiver antenna (FD 1×1, FD 2×1, HD 2×1, and HD 3×1), R1 was used as the receive antenna. For HD 2×2, R1 and R2 were used as receiver antennas. Further, if  $M$  antennas were required for transmission, we used  $T1$  to  $TM$ .

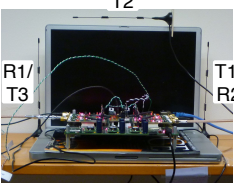
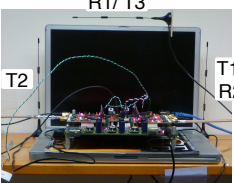
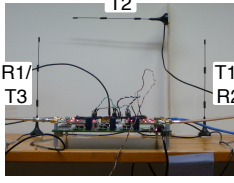
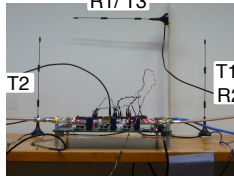
|             | Antenna Placement 1 (A1)  | Antenna Placement 2 (A2)   |
|-------------|---|--|
|             | T2 is orthogonal to T1<br>R1 is parallel to T1                                      | T2 is parallel to T1<br>R1 is orthogonal to T1                                       |
| With Device |  |  |
| No Device   |  |  |

Table 3.3: Four different antenna configurations used in experiments. The distance between parallel antennas is 37.5 cm. Antenna labels correspond to full-duplex and half-duplex antenna use. If  $M$  antennas are required for transmission we use  $T1$  to  $TM$ . If  $N$  antennas are required for reception we use  $R1$  to  $RN$ .

For the experiments with more than one transmitter antenna the multiple antenna codes used were the following. For the FD 2×1 experiments we used an Alamouti

code [14]. Hence, in Figure 2.2, the signals  $x_{i,1}$  and  $x_{i,2}$  correspond to Alamouti encoded symbols. The HD  $2 \times 1$  experiments also used an Alamouti code. The HD  $3 \times 1$  experiments used a rate  $3/4$  orthogonal space-time block code (OSTBC) from MATLAB MIMO library [15]. The HD  $2 \times 2$  experiments used spatial multiplexing for two spatial streams and the receive processing was implemented using channel inversion.

### 3.3 WARPLab Implementation

The digital and analog signal processing at a node were implemented using the WARPLab framework [16]. This framework facilitates experiment implementation by allowing the use of MATLAB for digital signal processing and the use of WARP [17] hardware for real-time over-the-air transmission and reception. In WARPLab, the baseband samples to be transmitted are generated in MATLAB and downloaded from MATLAB to transmit buffers inside the FPGA of the WARP hardware. Upon reception of a trigger (generated in the MATLAB session and communicated to the WARP hardware via Ethernet) the WARP hardware transmits the stored samples in real-time RF over-the-air. Also, upon reception of a trigger, any signal input to the receiver radio of a node is down converted from RF to baseband, the baseband signal is then converted from analog to digital domain and digital baseband samples of the received signal are stored in receive buffers in the FPGA. The received samples are uploaded from the FPGA to the MATLAB workspace for further signal processing.

All full-duplex and half-duplex experiments were conducted at a 2.4 GHz Wi-Fi channel without any other concurrent traffic. All systems implemented have a bandwidth of 20 MHz using 64 subcarriers with 48 subcarriers used for payload as in one of the possible Wi-Fi modes.

For each of the ten links considered, we ran experiments with both nodes using the

same antenna/device configuration and we considered all the possible combinations for the ten different links and four possible configurations shown in Table 3.3. This led to a total of 40 different scenarios. For each scenario we ran experiments for all the full-duplex and half-duplex systems listed in Table 3.2 and for four different transmission powers which were between -7 dBm and 8 dBm. For each scenario, transmission power used, and system tested, we transmitted 90 packets from each of the nodes in the link. Algorithm 1 shows the pseudocode for the WARPLab loop that controls transmission of packets for different transmission powers and systems evaluated in experiments. Algorithm 1 ran in approximately 10 hours. The reason for this duration is the latency of writing and reading large number of samples between the MATLAB workspace and the transmitter and receiver buffers in the WARP FPGA. For each of the 40 scenarios considered we ran Algorithm 1 twice hence we ran experiments for a total of 800 hours.

Each packet transmitted consisted of 68 OFDM symbols and each subcarrier was modulated using QSPK. Since there were 48 payload subcarriers per OFDM symbol, the total number of bits transmitted per packet per node was equal to 6528 and the total number of bits transmitted per node in 90 packets was equal to 587,520.

---

**Algorithm 1:** WARPLab loop for packet transmission.

---

```

for Packets 1 to 90 do
  for Transmit Powers 1 to 4 do
    for FD 2×1, HD 2×1, HD 3×1, HD 2×2, FD 1×1, HD 2×1, HD 1×1 do
      Transmit a packet from each of the two nodes in the link

```

---

### 3.4 Power and Self-Interference Cancellation Measurements for System Characterization

In this section we describe the power measurements that were made for characterization of our full-duplex device design and for comparison with half-duplex systems.

### 3.4.1 Transmitter Power

We use  $P_i$  to denote the transmission power of Node  $i$  and we use  $P_{i,j}$  to denote the transmission power of Node  $i$  transmitter antenna  $j$ . The total power transmitted by a node with  $M$  transmitter antennas, is given by

$$P_i = \sum_{j=1}^M P_{i,j}. \quad (3.1)$$

We characterized the transmission power of the WARP radios used in our experiments by connecting the radios directly to a spectrum analyzer. We also did a characterization using the RSSI measurements available on WARP radios. We observed that for an OFDM signal with 20 MHz bandwidth, all the radios used in experiments had a linear increase in transmit power as a function of the WARP transmitter gain settings for transmit powers up to 15 dBm. Increasing transmitter gains to achieve transmitter powers larger than 15 dBm would have been possible, however since some of our radios showed non linear behavior for output powers larger than 15 dBm, we only considered transmitter powers lower than 15 dBm. We note that for the same transmitter gain settings, the total power output by the radios varies as a function of the signal bandwidth. Consequently, our observations on the linear behavior of the radios are valid only for the 20 MHz bandwidth OFDM signals considered in our experiments.

Our characterization of the WARP radio transmission power as a function of the WARP radio transmitter gain settings allowed us to have an accurate measurement of the transmission powers used in our experiments.

### 3.4.2 Received Signal of Interest Power

All our experiments correspond to bidirectional communication between two nodes which we label as Node 1 and Node 2. We use  $P_{S,i}$  to denote the power of the signal of interest received at Node  $i$  and we use  $P_{S,i,j}$  to denote the power of the signal of interest received at Node  $i$  receiver antenna  $j$ . The total signal of interest power received by a node with  $N$  transmitter antennas, is given by

$$P_{S,i} = \sum_{j=1}^N P_{S,i,j}. \quad (3.2)$$

$P_{S,1}$  is measured when only Node 2 is transmitting and  $P_{S,2}$  is measured when only Node 1 is transmitting. In our experiments,  $P_{S,1}$  and  $P_{S,2}$  were computed based on the RSSI measurement of the WARP radios.

### 3.4.3 Received Self-Interference Power

The received self-interference power is equal to the self-interference power after passive cancellation and before active cancellation. We use  $P_{I,i}$  to denote the power of the self-interference received at Node  $i$ .  $P_{I,i}$  is measured when only Node  $i$  is transmitting. In our experiments,  $P_{I,i}$  was computed based on the RSSI measurement of the WARP radios.

### 3.4.4 Self-Interference Power after Passive and Analog Cancellation

We use  $P_{IAC,i}$  to denote the power of the self interference at Node  $i$  after passive and analog cancellation and before digital cancellation.  $P_{IAC,i}$  is measured when only Node  $i$  is transmitting. In our experiments,  $P_{IAC,i}$  was computed based on the RSSI measurement of the WARP radios.

### 3.4.5 Self-Interference Power after Passive, Analog, and Digital Cancellation

We use  $P_{\text{SIACDC},i}$  to denote the power of received signal of interest plus self-interference after passive, analog, and digital cancellation.  $P_{\text{SIACDC},i}$  is measured when both Node 1 and Node 2 are transmitting since  $P_{\text{SIACDC},i}$  is a measure of the signal of interest plus self-interference power. In our experiments,  $P_{\text{SIACDC},i}$  was computed based on the RSSI measurement of the WARP radios after passive and analog cancellation and the signal energy after digital cancellation. We computed the power of the self interference at Node  $i$  after passive, analog, and digital cancellation as follows,

$$P_{\text{IACDC},i} = P_{\text{SIACDC},i} - P_{\text{S},i} \quad (3.3)$$

Computing  $P_{\text{IACDC},i}$  as in Equation 3.3 was useful in order to reduce overhead which would have been required if  $P_{\text{IACDC},i}$  would have been measured directly with only Node  $i$  transmitting. This reduction in overhead will be explained in Section 3.5.1 when we present the time diagram per packet transmitted.

### 3.4.6 Amount of Cancellation

The amount of cancellation for the different cancellation mechanisms considered in our full-duplex device design can be computed using the power measurements described in Sections 3.4.1 to 3.4.5. The amount of dB of passive suppression at Node  $i$ ,  $\alpha_{\text{PS},i}$ , is computed as

$$\alpha_{\text{PS},i} \text{ (dB)} = P_i \text{ (dBm)} - P_{\text{I},i} \text{ (dBm)}. \quad (3.4)$$

The amount of dB of active (analog and digital) cancellation at Node  $i$ ,  $\alpha_{\text{ACDC},i}$ , is computed as

$$\alpha_{\text{ACDC},i} \text{ (dB)} = P_{\text{I},i} \text{ (dBm)} - P_{\text{IACDC},i} \text{ (dBm)}. \quad (3.5)$$

The amount of dB of active analog cancellation at Node  $i$ ,  $\alpha_{AC,i}$ , is computed as

$$\alpha_{AC,i} \text{ (dB)} = P_{I,i} \text{ (dBm)} - P_{IAC,i} \text{ (dBm)}, \quad (3.6)$$

and the amount of dB of active digital cancellation at Node  $i$ ,  $\alpha_{DC,i}$ , is computed as

$$\alpha_{DC,i} \text{ (dB)} = P_{IAC,i} \text{ (dBm)} - P_{IACDC,i} \text{ (dBm)}, \quad (3.7)$$

The total cancellation at Node  $i$ ,  $\alpha_{TOT,i}$ , is computed as

$$\alpha_{TOT,i} \text{ (dB)} = P_i \text{ (dBm)} - P_{IACDC,i} \text{ (dBm)}, \quad (3.8)$$

### 3.4.7 Block Diagram Showing a Subset of Power Measurements for a Full-duplex 2×1 Node

A block diagram of a full-duplex 2×1 node was shown in Figure 2.2. A block diagram of a full-duplex 2×1 node highlighting the locations where  $P_{i,1}$ ,  $P_{i,2}$ ,  $P_{S,i}$ ,  $P_{I,i}$ , and  $P_{IAC,i}$  were measured is shown in Figure 3.2. The WARP Rx Radio RSSI measurement was used to compute  $P_{S,i}$ ,  $P_{I,i}$ , and  $P_{IAC,i}$ . The signal  $\mathbf{z}_{i,n}$  was set equal to zero when  $P_{S,i}$  or  $P_{I,i}$  were being measured. When  $P_{IAC,i}$  was being measured the signal  $\mathbf{z}_{i,n}$  was used for analog cancellation. Analog cancellation was implemented as described in Section 2.2.

## 3.5 Time Diagram of a Packet

In this section we present the time diagram for transmission of a packet for a full-duplex 2×1 system and for a half-duplex 3×1 system. We explain the overhead sent for channel estimation and power measurements per packet. The time diagrams for other full-duplex and half-duplex systems implemented (full-duplex 1×1, half-duplex 2×1, and half-duplex 2×2) will not be presented since they can be obtained via straightforward modifications to the time diagrams for full-duplex 2×1 and half-duplex 3×1 systems.

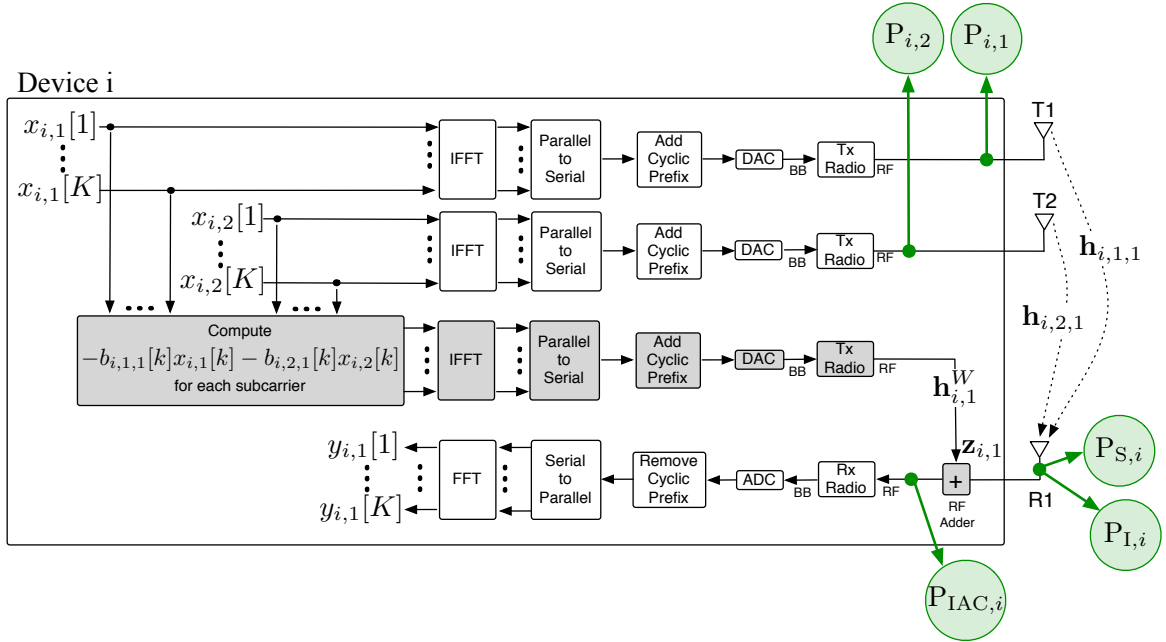


Figure 3.2: Block diagram of a full-duplex  $2 \times 1$  node using passive suppression and analog self-interference cancellation. Locations where  $P_{i,1}$ ,  $P_{i,2}$ ,  $P_{S,i}$ ,  $P_{I,i}$ , and  $P_{IAC,i}$  were measured are highlighted in green circles. Blocks used for active analog cancellation are highlighted in gray. Passive suppression consists in propagation loss through wireless self-interference channels  $\mathbf{h}_{i,1,1}$  and  $\mathbf{h}_{i,2,1}$ .

### 3.5.1 Time Diagram for a Full-duplex $2 \times 1$ Packet

A simplified block diagram representing the communication between two full-duplex  $2 \times 1$  nodes is shown in Figure 3.3. Each of the nodes corresponds to a full-duplex  $2 \times 1$  device implemented as described in Chapter 2. A more detailed block diagram for a full-duplex  $2 \times 1$  node was shown in Figure 2.2. The simplified block diagram in Figure 3.3 will be used to explain the time diagram of a packet for a full-duplex  $2 \times 1$  system.

In Figure 3.3 we use  $\mathbf{x}_{i,m}$  to denote the signal transmitted from Node  $i$  transmitter antenna  $m$ , and we use  $\mathbf{c}_i$  to denote the signal used for analog cancellation at Node  $i$ . The received signal at Node  $i$  is denoted as  $\mathbf{y}_{i,1}$ . The self-interference channel at

Node  $i$  between transmitter antenna  $m$  and the single receiver antenna is labeled as  $\mathbf{h}_{i,m,1}$ . The signal of interest channel between Node  $i$  transmitter antenna  $m$  and Node  $j$  single receiver antenna is labeled as  $\mathbf{h}_{S,i,j,m}$ . The wire channel for the analog canceller signal at Node  $i$  is labeled as  $\mathbf{h}_{i,1}^W$ .

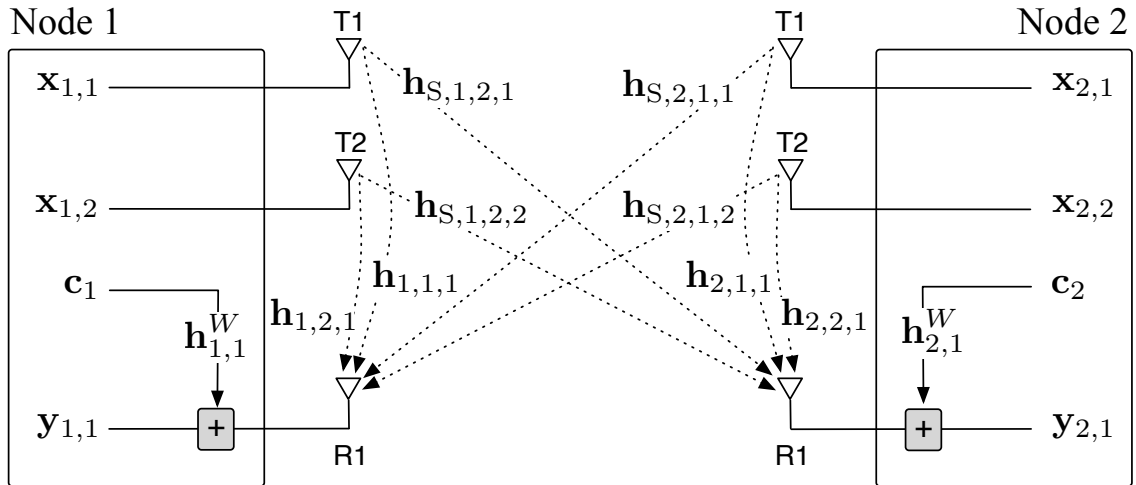


Figure 3.3: Simplified block diagram of a full-duplex  $2 \times 1$  system.

Figure 3.4 shows the time diagram for the signals transmitted during a full-duplex  $2 \times 1$  packet. Signals labeled as AT correspond to transmission of training used by the Automatic Gain Control (AGC) at the receiver radios. Signals labeled as PIL correspond to transmission of pilots used for channel estimation. Signals labeled as AC correspond to transmission (not wireless but locally via a wire) of the signal used for analog cancellation. Signals labeled as PAY correspond to transmission of payload. Time slots shaded in red correspond to transmissions that are used only for power measurements and system characterization but are not required to enable full-duplex  $2 \times 1$  communication. The time diagram is divided into 16 time slots which we label as  $\Lambda_1, \Lambda_2, \dots, \Lambda_{16}$ . The duration of each time slot is shown in Figure 3.4 in parenthesis. The signals transmitted and measured during each time slot are explained below.

- Time Slot  $\Lambda_1$

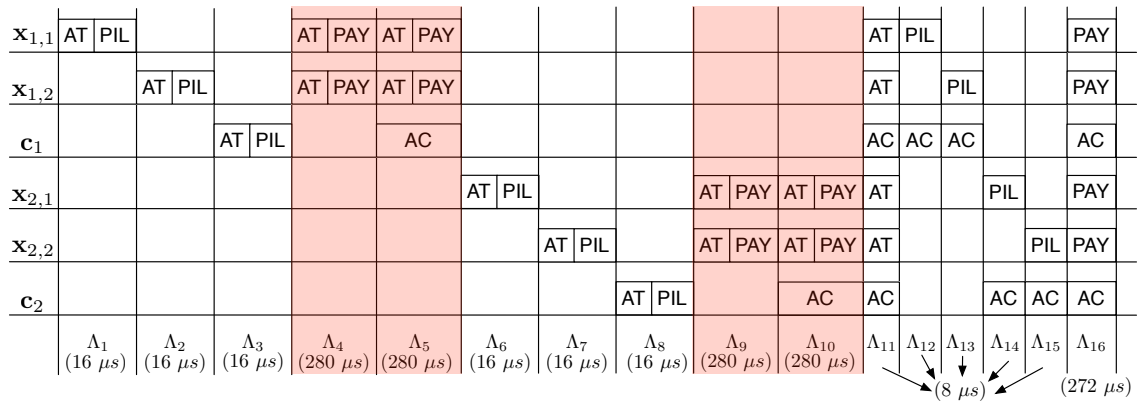


Figure 3.4: Time diagram for a full-duplex  $2 \times 1$  packet. The time diagram is divided into 16 time slots labeled  $\Lambda_1, \Lambda_2, \dots, \Lambda_{16}$ . The duration of each time slot is shown in parenthesis. Time slots shaded in red correspond to transmissions that are used only for power measurements and system characterization but are not required to enable full-duplex  $2 \times 1$  communication.

Node 1 T1 transmits training for AGC and pilots for channel estimation. The signal received at Node 1 is used for estimation of the self-interference channel  $\mathbf{h}_{1,1,1}$ .

- Time Slot  $\Lambda_2$

Node 1 T2 transmits training for AGC and pilots for channel estimation. The signal received at Node 1 is used for estimation of the self-interference channel  $\mathbf{h}_{1,2,1}$ .

- Time Slot  $\Lambda_3$

Node 1 transmits training for AGC and pilots for channel estimation via the analog canceller path. The signal received at Node 1 is used for estimation of the wire channel  $\mathbf{h}_{1,1}^W$ .

- Time Slot  $\Lambda_4$

Node 1 transmits payload (OFDM Alamouti symbols) from both transmitter antennas. The signal received at Node 2 is used to compute the power of the

received signal of interest at Node 2. We denote this signal power as  $P_{S,2}$ . The signal received at Node 1 is used to compute the power of the received self-interference at Node 1 after passive suppression (before active cancellation). We denote this signal power as  $P_{I,1}$ . The amount of passive suppression at Node 1 is computed as  $\alpha_{PS,1}$  (dB) =  $P_1$  (dBm) -  $P_{I,1}$  (dBm), where  $P_1$  is the transmission power of Node 1.

- Time Slot  $\Lambda_5$

Node 1 transmits payload (OFDM Alamouti symbols) from both transmitter antennas and signal  $\mathbf{c}_1$  is activated for analog cancellation of the self-interference at Node 1. Notice that the channel estimates required for self-interference cancellation at Node 1 were computed during time slots  $\Lambda_1$ ,  $\Lambda_2$ , and  $\Lambda_3$ . The signal received at Node 1 is used to compute the power of the received self-interference at Node 1 after passive suppression and analog cancellation (before digital cancellation). We denote this signal power as  $P_{IAC,1}$ . The amount of analog cancellation at Node 1 is computed as  $\alpha_{AC,1}$  (dB) =  $P_{I,1}$  (dBm) -  $P_{IAC,1}$  (dBm).

- Time Slot  $\Lambda_6$

Node 2 T1 transmits training for AGC and pilots for channel estimation. The signal received at Node 2 is used for estimation of the self-interference channel  $\mathbf{h}_{2,1,1}$ .

- Time Slot  $\Lambda_7$

Node 2 T2 transmits training for AGC and pilots for channel estimation. The signal received at Node 2 is used for estimation of the self-interference channel  $\mathbf{h}_{2,2,1}$ .

- Time Slot  $\Lambda_8$

Node 2 transmits training for AGC and pilots for channel estimation via the analog canceller path. The signal received at Node 2 is used for estimation of the wire channel  $\mathbf{h}_{2,1}^W$ .

- Time Slot  $\Lambda_9$

Node 2 transmits payload (OFDM Alamouti symbols) from both transmitter antennas. The signal received at Node 1 is used to compute the power of the received signal of interest at Node 1. We denote this signal power as  $P_{S,1}$ . The signal received at Node 2 is used to compute the power of the received self-interference at Node 2 after passive suppression (before active cancellation). We denote this signal power as  $P_{I,2}$ . The amount of passive suppression at Node 2 is computed as  $\alpha_{PS,2}$  (dB) =  $P_2$  (dBm) –  $P_{I,2}$  (dBm), where  $P_2$  is the transmission power of Node 2.

- Time Slot  $\Lambda_{10}$

Node 2 transmits payload (OFDM Alamouti symbols) from both transmitter antennas and signal  $\mathbf{c}_2$  is activated for analog cancellation of the self-interference at Node 2. Notice that the channel estimates required for self-interference cancellation at Node 2 were computed during time slots  $\Lambda_6$ ,  $\Lambda_7$ , and  $\Lambda_8$ . The signal received at Node 2 is used to compute the power of the received self-interference at Node 2 after passive suppression and analog cancellation (before digital cancellation). We denote this signal power as  $P_{IAC,2}$ . The amount of analog cancellation at Node 2 is computed as  $\alpha_{AC,2}$  (dB) =  $P_{I,2}$  (dBm) –  $P_{IAC,2}$  (dBm).

- Time Slot  $\Lambda_{11}$

All transmitters send training for AGC. Signal  $\mathbf{c}_1$  is activated for analog cancellation of the self-interference at Node 1 and signal  $\mathbf{c}_2$  is activated for analog

cancellation of the self-interference at Node 2. At both nodes, the received signal is used to set AGC gains which will be fixed during the remaining duration of the packet.

- Time Slot  $\Lambda_{12}$

Node 1 T1 transmits pilots for channel estimation and signal  $\mathbf{c}_1$  is activated for analog cancellation of the self-interference at Node 1. The signal received at Node 1 after passive and analog cancellation is used for estimation of the equivalent self-interference channel from T1 after passive and analog cancellation. This estimate is used for digital cancellation of the self-interference from T1 during the remaining duration of the packet. The signal received at Node 2 is used for estimation of the signal of interest channel  $\mathbf{h}_{S,1,2,1}$ .

- Time Slot  $\Lambda_{13}$

Node 1 T2 transmits pilots for channel estimation and signal  $\mathbf{c}_1$  is activated for analog cancellation of the self-interference at Node 1. The signal received at Node 1 after passive and analog cancellation is used for estimation of the equivalent self-interference channel from T2 after passive and analog cancellation. This estimate is used for digital cancellation of the self-interference from T2 during the remaining duration of the packet. The signal received at Node 2 is used for estimation of the signal of interest channel  $\mathbf{h}_{S,1,2,2}$ .

- Time Slot  $\Lambda_{14}$

Node 2 T1 transmits pilots for channel estimation and signal  $\mathbf{c}_2$  is activated for analog cancellation of the self-interference at Node 2. The signal received at Node 2 after passive and analog cancellation is used for estimation of the equivalent self-interference channel from T1 after passive and analog cancellation. This estimate is used for digital cancellation of the self-interference from

T1 during the remaining duration of the packet. The signal received at Node 1 is used for estimation of the signal of interest channel  $\mathbf{h}_{S,2,1,1}$ .

- Time Slot  $\Lambda_{15}$

Node 2 T2 transmits pilots for channel estimation and signal  $\mathbf{c}_2$  is activated for analog cancellation of the self-interference at Node 2. The signal received at Node 2 after passive and analog cancellation is used for estimation of the equivalent self-interference channel from T2 after passive and analog cancellation. This estimate is used for digital cancellation of the self-interference from T2 during the remaining duration of the packet. The signal received at Node 1 is used for estimation of the signal of interest channel  $\mathbf{h}_{S,2,1,2}$ .

- Time Slot  $\Lambda_{16}$

Node 1 and Node 2 transmit payload (OFDM Alamouti symbols) from both transmitter antennas. Signal  $\mathbf{c}_1$  is activated for analog cancellation of the self-interference at Node 1 and signal  $\mathbf{c}_2$  is activated for analog cancellation of the self-interference at Node 2.

The signal received at Node 1 is used to compute  $\text{SINR}_1$  which is the post processing (post Alamouti combining) SINR for full-duplex transmission from Node 2 to Node 1. The signal received at Node 1 is also used to compute the power of the received signal of interest plus self-interference after passive, analog, and digital cancellation at Node 1. We denote this signal power as  $P_{\text{SIACDC},1}$ . The power (in mW) of the self-interference at Node 1 after passive, analog, and digital cancellation is computed as  $P_{\text{IACDC},1} = P_{\text{SIACDC},1} - P_{S,1}$ . Notice that this way of computing  $P_{\text{IACDC},1}$  (as also shown in Equation 3.3), allows us to avoid transmitting another round of payload that would have been used only for measurement of digital cancellation.

The signal received at Node 2 is used to compute  $\text{SINR}_2$  which is the post processing (post Alamouti combining) SINR for full-duplex transmission from Node 1 to Node 2. The signal received at Node 2 is also used to compute the power of the received signal of interest plus self-interference after passive, analog, and digital cancellation at Node 2. We denote this signal power as  $P_{\text{SIACDC},2}$ . The power (in mW) of the self-interference at Node 2 after passive, analog, and digital cancellation is computed as  $P_{\text{IACDC},2} = P_{\text{SIACDC},2} - P_{\text{S},2}$ . Notice that this way of computing  $P_{\text{IACDC},2}$  (as also shown in Equation 3.3), allows us to avoid transmitting another round of payload that would have been used only for measurement of digital cancellation.

The amount of digital cancellation at Node 1 and Node 2 is computed as  $\alpha_{\text{DC},1} \text{ (dB)} = P_{\text{IAC},1} \text{ (dBm)} - P_{\text{IACDC},1} \text{ (dBm)}$  and  $\alpha_{\text{DC},2} \text{ (dB)} = P_{\text{IAC},2} \text{ (dBm)} - P_{\text{IACDC},2} \text{ (dBm)}$  respectively. The amount of active cancellation at Node 1 and Node 2 is computed as  $\alpha_{\text{ACDC},1} \text{ (dB)} = P_{\text{I},1} \text{ (dBm)} - P_{\text{IACDC},1} \text{ (dBm)}$  and  $\alpha_{\text{ACDC},2} \text{ (dB)} = P_{\text{I},2} \text{ (dBm)} - P_{\text{IACDC},2} \text{ (dBm)}$  respectively. The amount of total cancellation at Node 1 and Node 2 is computed as  $\alpha_{\text{TOT},1} \text{ (dB)} = P_1 \text{ (dBm)} - P_{\text{IACDC},1} \text{ (dBm)}$  and  $\alpha_{\text{TOT},2} \text{ (dB)} = P_2 \text{ (dBm)} - P_{\text{IACDC},2} \text{ (dBm)}$  respectively.

### 3.5.2 Time Diagram for a Half-duplex 3×1 Packet

A block diagram representing the communication between two half-duplex 3×1 nodes is shown in Figure 3.5. Each of the nodes corresponds to a half-duplex 3×1 device. The block diagram in Figure 3.5 will be used to explain the time diagram of a packet for a half-duplex 3×1 system. In Figure 3.5 we use  $\mathbf{x}_{i,m}$  to denote the signal transmitted from Node  $i$  transmitter antenna  $m$ . The received signal at Node  $i$  is denoted as  $\mathbf{y}_{i,1}$  and the signal of interest channel between Node  $i$  transmitter antenna

$m$  and Node  $j$  single receiver antenna is labeled as  $\mathbf{h}_{S,i,j,m}$ .

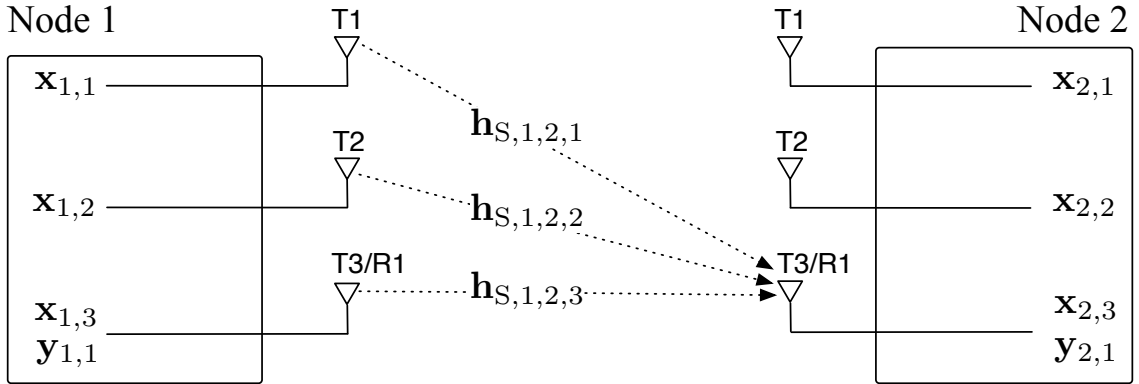


Figure 3.5: Simplified block diagram of a half-duplex  $3 \times 1$  system. The diagram shows the wireless channels between the transmitter antennas at Node 1 and the single receiver antenna at Node 2.

Figure 3.6 shows the time diagram for a half-duplex  $3 \times 1$  packet from Node 1 to Node 2 and a half-duplex  $3 \times 1$  packet from Node 2 to Node 1. As in figure 3.4, signals labeled as AT correspond to transmission of training used by the Automatic Gain Control (AGC) at the receiver radios, signals labeled as PIL correspond to transmission of pilots used for channel estimation, and signals labeled as PAY correspond to transmission of payload. The time diagram is divided into 10 time slots which we label as  $\Lambda_1, \Lambda_2, \dots, \Lambda_{10}$ . The duration of each time slot is shown in Figure 3.6 in parenthesis. The signals transmitted and measured during each time slot are explained below.

- Time Slot  $\Lambda_1$

Node 1 sends training for AGC from all its transmitter antennas. The signal received at Node 2 is used to set AGC gains which will be fixed during the remaining duration of the packet transmission from Node 1.

- Time Slot  $\Lambda_2$

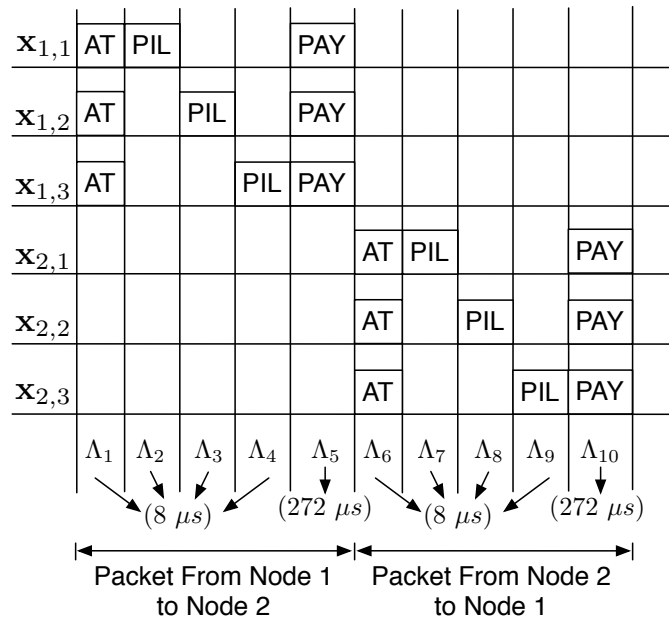


Figure 3.6: Time diagram for a half-duplex  $3 \times 1$  packet from Node 1 to Node 2 and a half-duplex  $3 \times 1$  packet from Node 2 to Node 1. The time diagram is divided into 10 time slots labeled  $\Lambda_1, \Lambda_2, \dots, \Lambda_{10}$ . The duration of each time slot is shown in parenthesis.

Node 1 T1 transmits pilots for channel estimation. The signal received at Node 2 is used for estimation of the signal of interest channel  $\mathbf{h}_{S,1,2,1}$ .

- Time Slot  $\Lambda_3$

Node 1 T2 transmits pilots for channel estimation. The signal received at Node 2 is used for estimation of the signal of interest channel  $\mathbf{h}_{S,1,2,2}$ .

- Time Slot  $\Lambda_4$

Node 1 T3 transmits pilots for channel estimation. The signal received at Node 2 is used for estimation of the signal of interest channel  $\mathbf{h}_{S,1,2,3}$ .

- Time Slot  $\Lambda_5$

Node 1 transmits payload (OFDM STBC symbols) from all the transmitter antennas. The signal received at Node 2 is used to compute  $\text{SINR}_2$  which is the

post processing (post OSTBC combining) SINR for half-duplex transmission from Node 1 to Node 2. The signal received at Node 2 is also used to compute the power of the received signal of interest at Node 2 ( $P_{S,2}$ ).

- Time Slot  $\Lambda_6$

Node 2 sends training for AGC from all its transmitter antennas. The signal received at Node 1 is used to set AGC gains which will be fixed during the remaining duration of the packet transmission from Node 2.

- Time Slot  $\Lambda_7$

Node 2 T1 transmits pilots for channel estimation. The signal received at Node 1 is used for estimation of the signal of interest channel  $\mathbf{h}_{S,2,1,1}$ .

- Time Slot  $\Lambda_8$

Node 2 T2 transmits pilots for channel estimation. The signal received at Node 1 is used for estimation of the signal of interest channel  $\mathbf{h}_{S,2,1,2}$ .

- Time Slot  $\Lambda_9$

Node 2 T3 transmits pilots for channel estimation. The signal received at Node 1 is used for estimation of the signal of interest channel  $\mathbf{h}_{S,2,1,3}$ .

- Time Slot  $\Lambda_{10}$

Node 2 transmits payload (OFDM STBC symbols) from all the transmitter antennas. The signal received at Node 1 is used to compute  $\text{SINR}_1$  which is the post processing (post OSTBC combining) SINR for half-duplex transmission from Node 2 to Node 1. The signal received at Node 1 is also used to compute the power of the received signal of interest at Node 1 ( $P_{S,1}$ ).

# Characterization of the Self-interference Cancellation

---

We have implemented our proposed self-interference cancellation mechanism which combines passive suppression and active cancellation techniques. In this Chapter we present a characterization of the cancellations achieved.

## 4.1 Passive Suppression

The amount of passive suppression is computed as shown in Equation 3.4. In our experiments we computed the amount of passive suppression at a node for each full-duplex packet transmitted. Figure 4.1 shows a characterization of the amount of passive suppression achieved by the four different configurations listed in Table 3.3. First, we observe that at a CDF value of 0.5, configuration A1 with device achieves approximately 10 dB better cancellation than A1 without device. Similarly, at a CDF value of 0.5, configuration A2 with device is observed to achieve approximately 10 dB better cancellation than A2 without device. Hence, we conclude that placing antennas around a device improves the passive suppression by approximately 10 dB.

Second, we observe that at a CDF value of 0.5 configuration A2 with device achieves approximately 5 dB better cancellation than A1 with device. Similarly, A2 without device achieves approximately 5 dB better cancellation than A1 without device. Hence, we conclude that antenna placement A2 improves the passive suppression by approximately 5 dB with respect to antenna placement A1. The reason for this improvement is due to the fact that in A2 the receiver antenna main lobe is placed orthogonal with respect to the transmitter antennas main lobe. Consequently,

A1 results in less coupling between self-interfering antennas and this results in larger levels of passive suppression.

Recent characterizations of passive suppression mechanisms [4, 6] for multiple transmitter antennas demonstrate levels of passive suppression lower than 60 dB. Our results in Figure 4.1 show that taking into account the antenna pattern and placing the antennas around the full-duplex device serves as further means of passive suppression and helps achieve passive suppression values between 60 dB and 70 dB.

Furthermore, we note that out of the four different configurations considered, A2 with device is not only the best suited for full-duplex communications but it is also well suited for half-duplex communications with multiple antennas. This is because multiple antenna communications benefit from independent channels from different antennas and placing antennas around a device with orthogonal patterns helps achieving independent channels from different antennas.

We note from Figure 4.1 that our analysis of passive suppression holds for both FD  $2 \times 1$  and FD  $1 \times 1$  systems.

## 4.2 Active Analog and Digital Cancellation

The amount of active cancellation (achieved by combining active analog with active digital cancellation) is computed as shown in Equation 3.5. In our experiments we computed the amount of active cancellation at a node for each full-duplex packet transmitted. Figure 4.2 shows a characterization of the amount of active cancellation achieved. We observe that configurations A1 with device and A2 with device achieve the lowest levels of active cancellation and configurations A1 without device and A2 without device achieve the largest levels of active cancellation. Hence, the roles for best/worse cancellation out of the four configurations considered have inverted with respect to the passive suppression performance reported in Figure 4.1. In Figure 4.1,

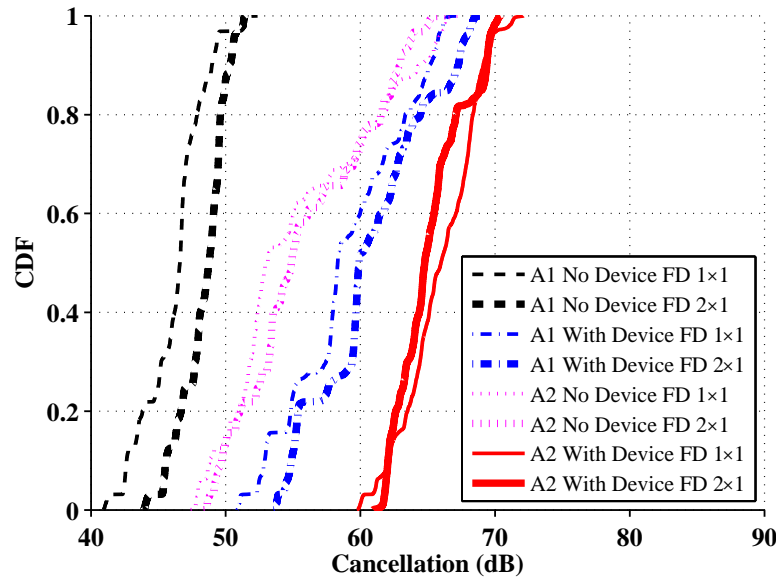


Figure 4.1: CDF of passive suppression.

the best performance was achieved by the configurations with device and the worse performance was achieved by the configurations without device.

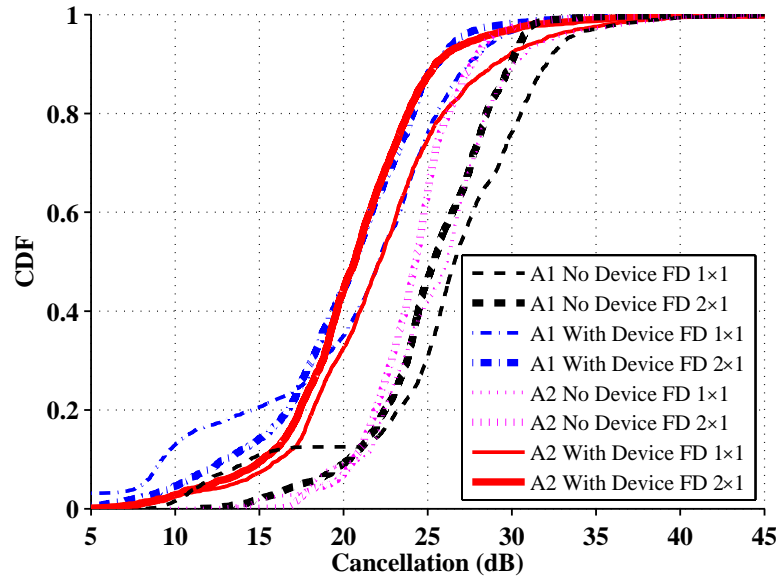


Figure 4.2: CDF of active (analog + digital) cancellation.

The reason why configurations with device achieve the lowest levels of active cancellation is because active cancellation is based on an estimate of the self-interference

channel. The weaker the received self-interference (self-interference at the receiver antenna) the worse the estimate of the self-interfering channel and the worse the amount of active cancellation achieved. Configurations with device have the weakest levels of received self-interference because they achieve the largest passive suppression.

Figure 4.3 shows the amount of active cancellation  $\alpha_{\text{ACDC},i}$  as a function of the received self-interference power  $P_{\text{I},i}$  (self-interference power before active cancellation) for a full-duplex  $1 \times 1$  and a full-duplex  $2 \times 1$  system. Results shown in Figure 4.3(a) and Figure 4.3(b) correspond to a scatter plot of per packet measurements and a linear fit of the scatter plot data. Different markers correspond to different antenna/device configurations. The scatter plot and linear fit of the data shown in Figure 4.3 verify that for FD  $1 \times 1$  and FD  $2 \times 1$  systems, the amount of active cancellation increases as the received self interference power increases.

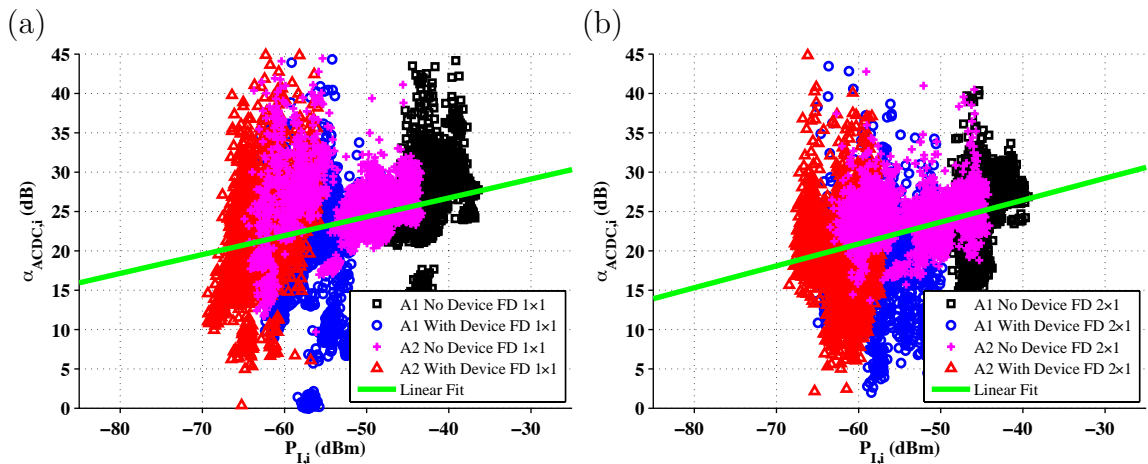


Figure 4.3: Amount of active cancellation  $\alpha_{\text{ACDC},i}$  as a function of the received self-interference power  $P_{\text{I},i}$  (self-interference power before active cancellation). Different markers correspond to different antenna/device configurations (a). Results for full-duplex  $1 \times 1$ . (b). Results for full-duplex  $2 \times 1$ .

In summary, the reason for the behaviors observed in Figure 4.2 and Figure 4.3 is the following. *In order to implement active cancellation we first need to estimate the self-interference channel. As the power of the self-interference before active cancel-*

*lution increases, the noise in the estimation of the wireless self-interference channel decreases, and thus, the active cancellation process is more exact leading to larger suppression of the self-interference.*

We dig deeper into the relative contributions of analog and digital cancellation and find the following result. *As the performance of analog cancellation gets better, the effectiveness of digital cancellation after analog cancellation reduces.*

Experiment results in Figure 4.4 show the amount of digital cancellation  $\alpha_{DC,i}$  as a function of the amount of analog cancellation  $\alpha_{AC,i}$  for a full-duplex  $1 \times 1$  and a full-duplex  $2 \times 1$  system. Results shown in Figure 4.4(a) and Figure 4.4(b) correspond to a scatter plot of per packet measurements and a linear fit of the scatter plot data. Different markers correspond to different antenna/device configurations. The scatter plot and linear fit of the data shown in Figure 4.4 verify that for FD  $1 \times 1$  and FD  $2 \times 1$  systems, the amount of digital cancellation decreases as the amount of analog cancellation increases.

Intuitively it is clear that if analog cancellation can achieve perfect cancellation (infinite dB of cancellation) then digital cancellation is unnecessary. In fact, if analog cancellation can achieve perfect cancellation then applying digital cancellation after analog cancellation can result in an increase in the self-interference. This effect is a consequence of trying to cancel a signal that is not present in the received signal.

Figure 4.5 shows the probability that digital cancellation results in an increase in the total cancellation during a packet as a function of the amount of analog cancellation achieved during a packet. From results in Figure 4.5 we conclude the following. *The smaller the amount of analog cancellation during a packet, the larger the probability that applying digital cancellation after analog cancellation can increase the total self-interference cancellation during that packet.*

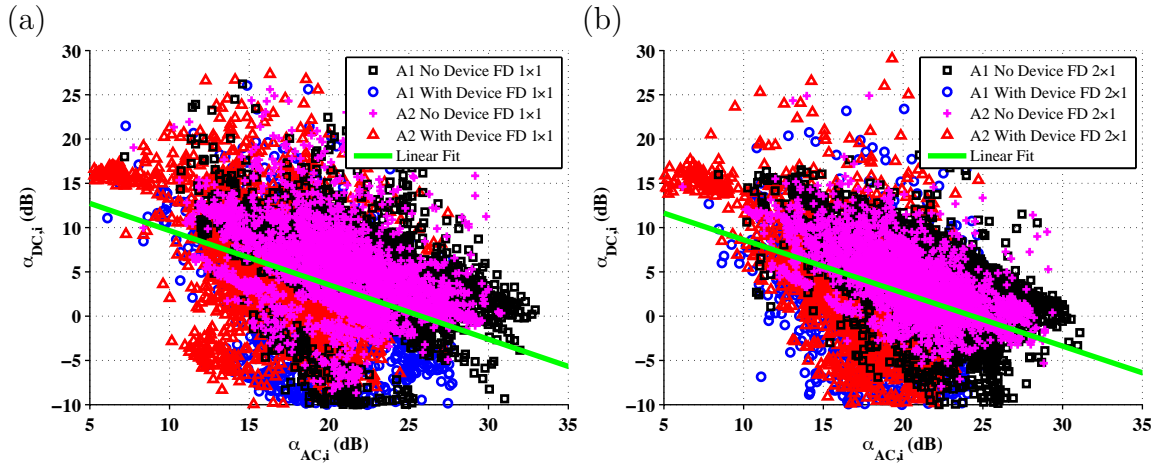


Figure 4.4: Amount digital cancellation  $\alpha_{DC,i}$  as a function of the amount of analog cancellation  $\alpha_{AC,i}$ . Different markers correspond to different antenna/device configurations (a). Results for full-duplex 1 $\times$ 1. (b). Results for full-duplex 2 $\times$ 1.

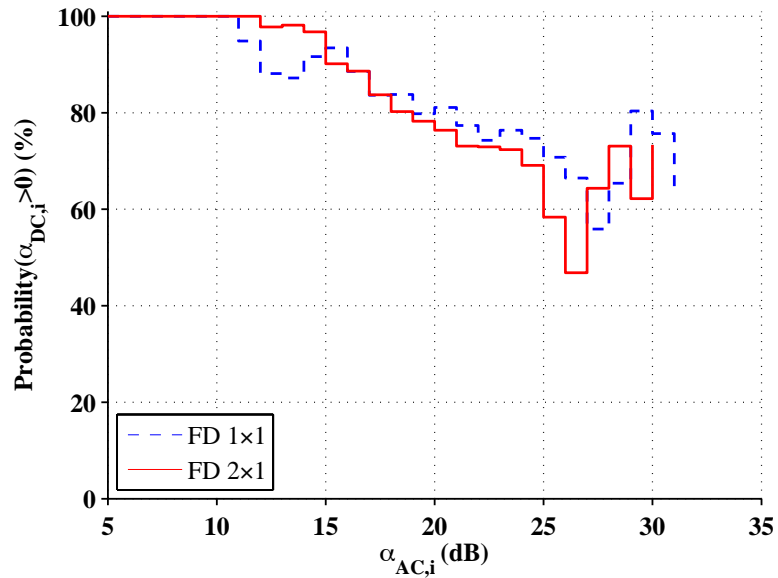


Figure 4.5: Probability that digital cancellation after analog cancellation increases the total amount of cancellation.

Previous work [5] had conjectured that the performance of digital cancellation is independent of the cancellation stages that precede it. Hence, previous work had assumed that if digital cancellation by itself (measured in isolation) can cancel up to 30 dB, then it would also cancel 30 dB when applied after analog cancellation. This conjecture is incorrect, as is demonstrated by our results in Figure 4.4 and Figure 4.5

which show that (a) applying digital cancellation after analog cancellation can sometimes increase the self-interference and (b) the effectiveness of digital cancellation in a full-duplex system will depend on the performance of the cancellation stages that precede it

We note that all our results presented so far are for 20 MHz wideband OFDM systems and the results presented in Figure 4.3, Figure 4.4 and Figure 4.5 are in agreement with results for narrowband FD  $1 \times 1$  systems presented in [18].

### 4.3 Total Cancellation

The amount of total cancellation is computed as shown in Equation 3.8. In our experiments we computed the amount of total cancellation at a node for each full-duplex packet transmitted. Figure 4.6 shows a characterization of the total cancellation achieved when combining passive suppression with active analog and active digital cancellation. Figure 4.6 shows results for the four different configurations listed Table 3.3. We observe that A2 with device achieves the largest total cancellation. Hence, although previously we observed that the active cancellation for A2 with device is one of the lowest among the configurations considered, the large amount of passive suppression achieved for A2 with device is such that this configuration achieves the largest total cancellation. The cancellation values for A2 with device for a full-duplex  $2 \times 1$  system are between 70 dB and 100 dB with an average of 85 dB.

We also note that although A1 without device achieved the largest amount of active cancellation, the total cancellation was the lowest due to the worse performance of passive suppression for this configuration. In general, we observe that for the same implementation of active analog and digital cancellation, the largest cancellation will be obtained with the configuration that achieves the largest passive suppression.

This leads to an important direction that *antenna design and placement* are crucial for achieving practical full-duplex, and the design has to be cognizant of the device dimensions and placement.

Finally, we observe that the performance of the cancellation scheme was very similar between the FD  $2\times 1$  and FD  $1\times 1$  systems.

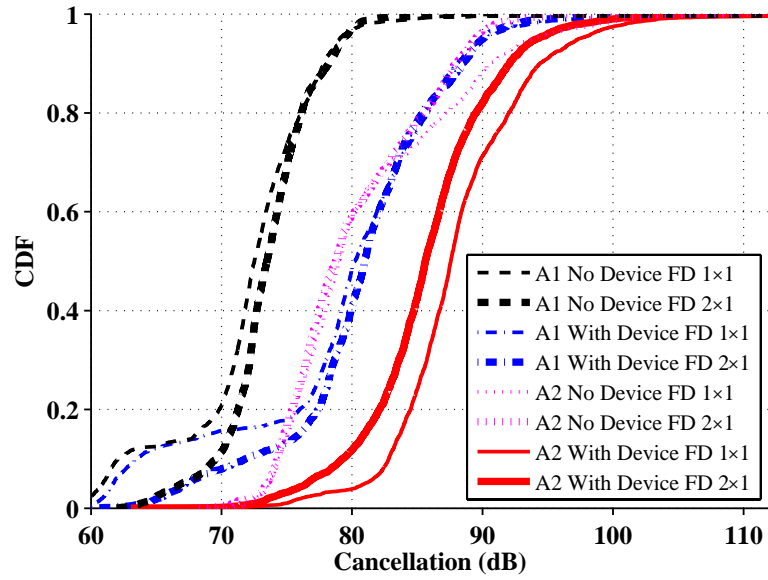


Figure 4.6: CDF of total cancellation.

# Full-duplex Ergodic Rates and Comparison with Half-duplex

---

This chapter presents an experiment based characterization of the rate performance of our full-duplex device design. We analyze the effects of self-interference cancellation on the rate performance of full-duplex systems and we demonstrate that our full-duplex device design can achieve full-duplex gains at Wi-Fi ranges.

## 5.1 Performance Metric: Empirical Ergodic Rates

The ergodic rate is the fundamental measure of physical layer capacity in fading channels [19] and is an upper bound on the throughput that would be achieved by any Media Access Control (MAC) protocol. The ergodic rates become the starting point for a system designer to choose actual constellation sizes and code rates. The Ergodic Rate (ER) for transmission to Node  $i$  is given by

$$\text{ER}_i = E[\log(1 + \text{SINR}_i[p])], \quad (5.1)$$

where the expected value is computed as the average over all the packets  $p$  transmitted to Node  $i$  and  $\text{SINR}_i[p]$  is the post processing Signal to Interference plus Noise Ratio (SINR) for packet  $p$  received at Node  $i$ . For a full-duplex two-way communication the Ergodic Sum Rate is computed as

$$\text{ESR} = \text{ER}_1 + \text{ER}_2. \quad (5.2)$$

The empirical ergodic rate in experiments is computed based on an estimate of  $\text{SINR}_i[p]$ . We estimate  $\text{SINR}_i[p]$  from transmitted and received constellation symbols

as follows. The constellation symbol  $s_i$  is sent to Node  $i$  via the wireless channel. Node  $i$  processes the received signal and computes  $\hat{s}_i$  which is the estimate of  $s_i$ . The average energy of the error is given by  $E[|s_i - \hat{s}_i|^2]$ . The post processing SINR for packet  $p$  received at node  $i$ ,  $\text{SINR}_i[p]$ , is computed as

$$\text{SINR}_i[p] = \frac{E[|s_i|^2]}{E[|s_i - \hat{s}_i|^2]}, \quad (5.3)$$

where the expected value is computed as the average over all the symbols transmitted to Node  $i$  during packet  $p$ . The achievable rate for transmission to Node  $i$  during packet  $p$  is given by

$$\text{AR}_i[p] = \log(1 + \text{SINR}_i[p]), \quad (5.4)$$

The empirical ergodic rate for transmission to Node  $i$  is computed by averaging the achievable rate over all the received packets as shown in Equation 5.1. In our experiments the symbols  $s_i$  were QPSK symbols. We note that the computation of  $\text{SINR}_i[p]$  is independent of the shape of the constellation used and depends only on the constellation energy  $E[|s_i|^2]$  [20].

## 5.2 Full-duplex Ergodic Rates with Increasing Power

Before presenting our rate analysis as a function of increasing power we first introduce the following useful notation. We use  $\text{SIR}_i$  to denote the Signal to Interference Ratio at Node  $i$  before active cancellation and we use  $\text{SIR}_{\text{ACDC},i}$  to denote the Signal to Interference Ratio at Node  $i$  after active cancellation.  $\text{SIR}_i$  is computed as

$$\text{SIR}_i = \frac{P_{\text{S},i}}{P_{\text{I},i}}, \quad (5.5)$$

where  $P_{\text{S},i}$  is the power of the signal of interest received at Node  $i$  and  $P_{\text{I},i}$  is the power of the self-interference received at Node  $i$  before active cancellation.  $\text{SIR}_{\text{ACDC},i}$  is computed as

$$\text{SIR}_{\text{ACDC},i} = \frac{P_{\text{S},i}}{P_{\text{IACDC},i}} = \frac{P_{\text{S},i}}{P_{\text{I},i}/\alpha_{\text{ACDC},i}} = \alpha_{\text{ACDC},i} \text{SIR}_i, \quad (5.6)$$

where  $P_{\text{IACDC},i}$  is the power of the self-interference at Node  $i$  after active (analog and digital) cancellation and  $\alpha_{\text{ACDC},i}$  is the amount of cancellation achieved by active (analog and digital) cancellation at Node  $i$ . Notice from Equation 5.6 that applying active cancellation increases the Signal to Interference Ratio by a factor of  $\alpha_{\text{ACDC},i}$ .

Our first rate result based on experimental data is as follows. *If the Signal to Interference Ratio before active cancellation at Node  $i$ ,  $\text{SIR}_i$ , is maintained constant while the received self-interference power at Node  $i$ ,  $P_{\text{I},i}$ , is increased, then the ergodic rate for transmission to Node  $i$  increases.* This result is verified by experiment results shown in Figure 5.1 where the ergodic rate for transmission to Node  $i$  is plotted as a function of the average received self-interference power at Node  $i$  (computed by averaging over all the received packets). Each curve in Figure 5.1 corresponds to an almost constant average  $\text{SIR}_i$  (computed by averaging over all the received packets). The solid line in Figure 5.1 shows the ergodic rates for transmission to Node  $i$  at average  $\text{SIR}_i$  values between -21.0 dB and -20.4 dB. The dashed line in Figure 5.1 shows the ergodic rates for transmission to Node  $i$  at average  $\text{SIR}_i$  values between -16.1 dB and -15.1 dB. The exact average  $\text{SIR}_i$  is shown in parenthesis next to each data point. For each curve in Figure 5.1 we observe that although the average value of  $\text{SIR}_i$  is approximately constant, the ergodic rate for transmission to Node  $i$  is increasing as  $P_{\text{I},i}$  increases.

The reasons for the behavior shown in Figure 5.1 are the following. The SINR at Node  $i$  after active cancellation is given by

$$\begin{aligned} \text{SINR}_{\text{ACDC},i} &= \frac{P_{\text{S},i}}{P_{\text{IACDC},i} + N_0} \\ &= \frac{P_{\text{S},i}}{P_{\text{I},i}/\alpha_{\text{IACDC}} + N_0} \\ &= 1 / \left( \frac{1}{\alpha_{\text{ACDC}} \text{SIR}_i} + \frac{1}{\text{SNR}_i} \right), \end{aligned} \quad (5.7)$$

where  $N_0$  is the noise power which is a result of the thermal noise in the receiver

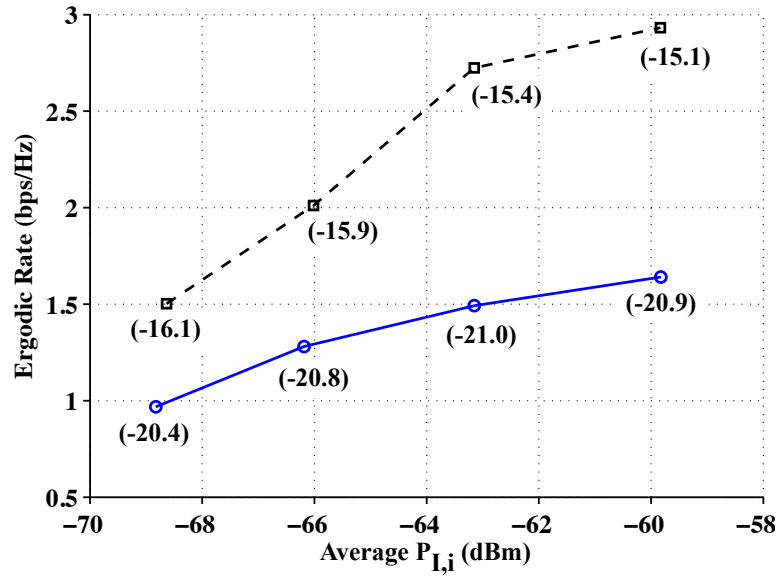


Figure 5.1: Experiment results showing the ergodic rate as a function of the average received self-interference power for an approximately constant value of average  $SIR_i$ . The exact value of average  $SIR_i$  for each data point is shown in parenthesis. Results correspond to a FD  $2 \times 1$  system. The dashed curve corresponds to measurements made at Node d for Link 7 and the solid curve corresponds to measurements made at Node d for Link 9. A description of each link and the node location was presented in Section 3.1.

circuitry and  $SNR_i$  is the Signal to Noise Ratio at Node  $i$ . Notice from Equation 5.5 that if  $SIR_i$  remains constant while  $P_{I,i}$  increases then this means that  $P_{S,i}$  is increasing and the rate of increase of  $P_{S,i}$  is the same rate of increase as  $P_{I,i}$ . Hence, if  $SIR_i$  remains constant while  $P_{I,i}$  increases then the terms in the equation for  $SINR_{ACDC,i}$  that are changing are  $\alpha_{ACDC}$  and  $SNR_i$  and they are both increasing (remember from Section 4.2 that as the received self-interference power  $P_{I,i}$  increases the amount of active cancellation  $\alpha_{ACDC}$  increases) consequently  $SINR_{ACDC,i}$  increases and this results in an increase in ergodic rate.

It is important to highlight that  $SINR_{ACDC,i}$  is computed after active cancellation but before applying any receiver combining (i.e. before applying any receiver combining like Alamouti combining or Maximum Ratio Combining (MRC)). Conse-

quently  $\text{SINR}_{\text{ACDC},i}$  is different from the post processing SINR in Equation 5.3. The post processing SINR in Equation 5.3 ( $\text{SINR}_i$ ) is computed based on the estimate of the transmitted symbols hence it is computed after applying receiver combining. Although  $\text{SINR}_{\text{ACDC},i}$  and  $\text{SINR}_i$  are different, and increase in  $\text{SINR}_{\text{ACDC},i}$  (SINR before receiver combining) will lead to an increase in  $\text{SINR}_i$  (SINR after receiver combining). Hence, an increase in  $\text{SINR}_{\text{ACDC},i}$  will lead to an increase in the ergodic rate.

From our analysis of results in Figure 5.1 we conclude the following. Consider two nodes, Node 1 and Node 2, communicating in full-duplex mode. If the transmission power at Node 1 and Node 2 is increased by the same amount then  $\text{SIR}_1$  and  $\text{SIR}_2$  will not change and  $P_{I,1}$  and  $P_{I,2}$  will increase hence, as can be concluded from our previous analysis, the ergodic rate in both directions of the full-duplex link will increase. Hence, our analysis leads to the following design rule for two-way full-duplex systems.

*Design Rule 1 (Rate-Power Increase):* In a two way full-duplex system, increasing the transmission power at both nodes by the same amount results in an increase of the ergodic rate in both directions of the link and this increases the ergodic sum rate of the full-duplex system.

Our *Design Rule 1* is verified by experiment results in Figure 5.2 which correspond to the case where the two nodes that are communicating via full-duplex use the same transmission power  $P$ . From Figure 5.2 we observe that as  $P$  increases the ergodic sum rate of the full-duplex link also increases.

Previous related work [3] has suggested that full-duplex communications can be improved by decreasing the transmission power. However, our results in Figure 5.2 demonstrate that there can be scenarios where increasing the transmission power results in higher full-duplex rates.

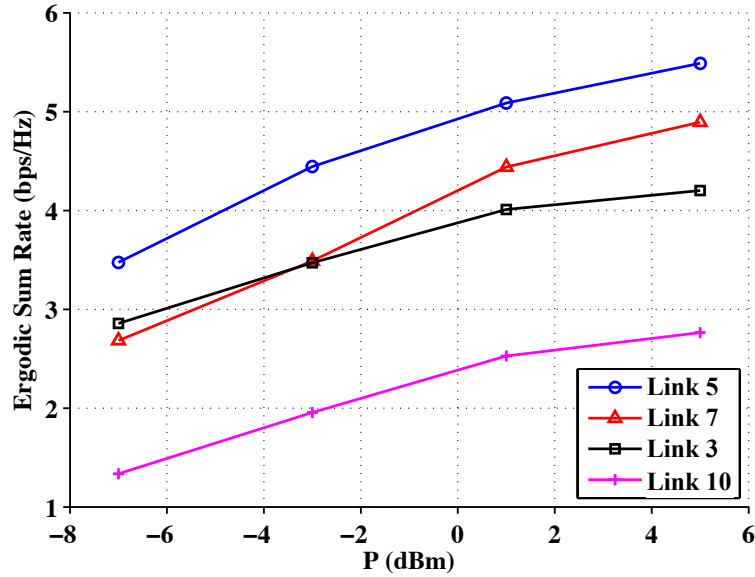


Figure 5.2: Experiment results showing an increase in the ergodic sum rate as a function of the transmission power for a full-duplex two-way system using the same transmission power at both nodes. Results are for a full-duplex  $2 \times 1$  system. A description of each link and the node location was presented in Section 3.1.

We note that all our results presented so far are for 20 MHz wideband OFDM systems and the results presented in Figure 5.1 and Figure 5.2 are in agreement with results for narrowband FD  $1 \times 1$  systems presented in [18].

### 5.3 Comparison of Full-duplex and Half-duplex Systems

#### 5.3.1 Power Assignment for Fair Comparison between Full-duplex and Half-duplex

For a fair comparison, the total energy transmitted by a full-duplex node must be the same as the total energy transmitted by a half-duplex node. Since energy is power times transmission time, the following equation defines the relationship between full- and half-duplex powers

$$P_i^{\text{FD}} T_i^{\text{FD}} = P_i^{\text{HD}} T_i^{\text{HD}}, \quad (5.8)$$

where  $P_i^{\text{FD}}$  denotes the transmission power use by Node  $i$  in full-duplex mode,  $P_i^{\text{HD}}$  denotes the transmission power used by Node  $i$  in half-duplex mode,  $T_i^{\text{FD}}$  denotes the duration of a transmission from Node  $i$  in full-duplex mode, and  $T_i^{\text{HD}}$  denotes the duration of a transmission from Node  $i$  in half-duplex mode.

Let  $\Pi$  denote the maximum power that can be radiated by the system (not just one node, but all the nodes in the system together) at any time. Since half-duplex transmissions from each node in a two-way link are orthogonal in time, it implies that  $P_1^{\text{HD}} \leq \Pi$  and  $P_2^{\text{HD}} \leq \Pi$ . In contrast, since full-duplex transmissions from each node in a two-way link are simultaneous, the instantaneous radiated power constraint of  $\Pi$  translates to a power constraint of  $P_1^{\text{FD}} + P_2^{\text{FD}} \leq \Pi$  for full-duplex nodes. Thus, we ensure that at any given time, a network with full-duplex nodes does not use more energy than a network with half-duplex nodes.

In any two-way communication, the amount of time for each direction can be controlled. Consider a finite duration,  $\tau$ , of time for bi-directional communication between Nodes 1 and 2. From time constraints for full-duplex and half-duplex we have that  $T_1^{\text{FD}} = T_2^{\text{FD}} = \tau$  and  $T_1^{\text{HD}} + T_2^{\text{HD}} = \tau$ . We define  $\beta = T_1^{\text{HD}}/\tau$ . Using Equation 5.8, the definition of  $\beta$ , and the time constraints, we obtain that for a fair comparison between full-duplex and half duplex systems the node powers used in full-duplex and half-duplex must satisfy  $P_1^{\text{FD}} = P_1^{\text{HD}}\beta$  and  $P_2^{\text{FD}} = P_2^{\text{HD}}(1 - \beta)$ .

For all our comparisons between full-duplex and half-duplex systems the power constraint was equal to  $\Pi = 8$  dBm and we achieved this constraint with equality. Hence, our experiments correspond to the following power assignments.  $P_1^{\text{HD}} = P_2^{\text{HD}} = 8$  dBm,  $P_1^{\text{FD}} = 8$  dBm +  $10 \log_{10}(\beta)$ , and  $P_2^{\text{FD}} = 8$  dBm +  $10 \log_{10}(1 - \beta)$ . We performed only symmetric experiments, where  $\beta = 0.5$ , leading to  $P_1^{\text{FD}} = P_2^{\text{FD}} = 5$  dBm.

Since the two-way communication in half-duplex is achieved by time sharing the link with a fraction of time  $1 - \beta$  dedicated for transmission to Node 1 and a fraction of time  $\beta$  dedicated for transmission to Node 2, the computation of ergodic rate for half-duplex transmission to a node has been scaled by the time of transmission. Consequently, the ergodic rate for transmission to Node 1 in a half-duplex system is equal to  $ER_1(1 - \beta)$  and the ergodic rate for transmission to Node 2 in a half-duplex system is equal to  $ER_2\beta$ , where rates  $ER_1$  and  $ER_2$  are computed based on the estimation of the post processing SINR during half-duplex communication. For a full-duplex system, since both nodes transmit at the same time, the ergodic rate for transmission to Node 1 is equal to  $ER_1$  and the ergodic rate for transmission to Node 2 is equal to  $ER_2$ , where rates  $ER_1$  and  $ER_2$  are computed based on the estimation of the post processing SINR during full-duplex communication.

### 5.3.2 Comparison of Full-duplex and Half-duplex Ergodic Rates

Previous implementations of self-interference cancellation designs report less than 80 dB of total cancellation with an average cancellation close to 73 dB [7, 4, 5]. These total cancellation values are similar to the ones achieved by configuration A1 without device as can be seen from Figure 4.6. Ergodic rate results for full-duplex and half-duplex systems using configuration A1 without device are shown in Figure 5.3. Specifically, Figure 5.3 shows the ergodic rate for transmission to a node in a two-way link as a function of the average signal of interest RSSI at the node. The average RSSI at a node was computed by averaging the received signal of interest power over all the 90 packets received during an experiment run. For each of the 90 packets received, the achievable rate per packet was computed as shown in Equation 5.4 and the ergodic rate was computed by averaging the achievable rate per packet over all the 90 packets received. Figure 5.3 shows the experiment results and the performance approximated by a linear fit of the experiment results.

The RSSI based description of the range can be translated into physical ranges (in meters), depending on the propagation losses encountered in different environments. Figure 5.3 also shows the ergodic rate versus range in meters for two widely used propagation models [9], where pathloss is given by  $40 \text{ dB} + 10n \log(l)$  where  $l$  is the distance between communicating nodes. The ranges in meters shown in Figure 5.3 are for unobstructed (line-of-sight) in-building conditions, which correspond to  $n = 1.7$ , and for severely attenuated obstructed (non-line-of-sight) indoor conditions, which correspond to  $n = 5$ . All schemes compared in Figure 5.3 utilize the same total power  $\Pi = 8 \text{ dBm}$ .

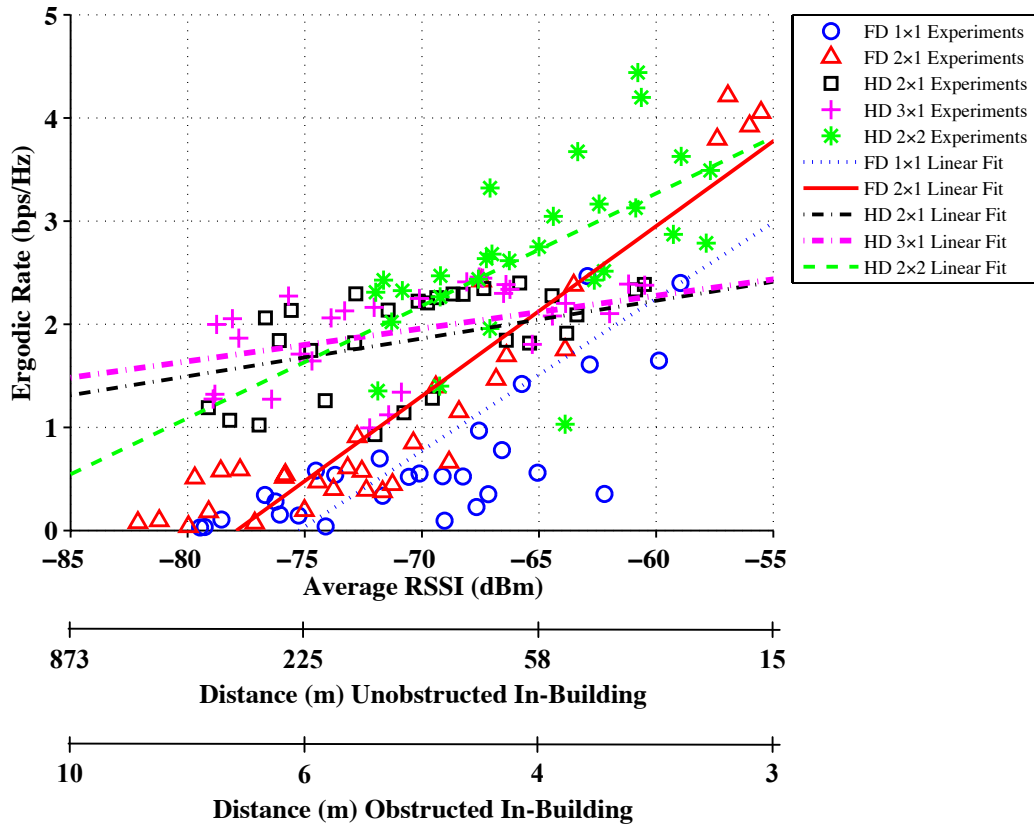


Figure 5.3: Ergodic rate vs. average RSSI for full-duplex and half-duplex systems. Results correspond to experiments performed with nodes using Antenna Placement A1 without a device.

Based on the linear fit of experiment data in Figure 5.3 we conclude the following.

A FD  $1 \times 1$  system with a self-interference cancellation design that achieves less than 80 dB cancellation with an average of 73 dB cancellation (as configuration A1 without device) will achieve better rates than half-duplex systems only at levels of signal of interest RSSI larger than  $-60$  dBm. Typical operation of Wi-Fi systems corresponds to RSSI values between  $-80$  dBm and  $-60$  dBm, hence, previously reported full-duplex single antenna implementations will not be able to achieve full-duplex gains in Wi-Fi ranges.

We observe from Figure 5.3 that full-duplex with two transmitter antennas helps improve performance due to the advantage of multiple antenna diversity. However, the performance of FD  $2 \times 1$  with antenna placement A1 without device is worse than half-duplex for RSSI values less than  $-65$  dBm. Hence, average cancellations larger than 73 dB are required for full-duplex operation over Wi-Fi RSSI ranges, which also explains why prior work could not achieve larger ranges.

We next report the performance of full-duplex and half-duplex systems using antenna configuration A2 with device. This is the configuration that achieves the largest total cancellations values (between 70 dB and 100 dB with an average of 85 dB) among the four configurations considered. Figure 5.4 demonstrates our main result: *using configuration A2 with device and our proposed active self-interference canceller design can achieve gains over half-duplex systems over a significant portion of the range of RSSI values typical of Wi-Fi operation.* Specifically, based on the linear fit of experiment data in Figure 5.4, we conclude that our FD  $2 \times 1$  implementation achieves 30–84% higher ergodic rates than HD  $3 \times 1$  for received powers in the range of  $[-75, -60]$  dBm. We also conclude that, compared to an HD  $2 \times 2$  system, our FD  $2 \times 1$  implementation achieves larger rates for RSSI values larger than  $-75$  dBm.

We note that our main result is obtained from an extensive characterization of

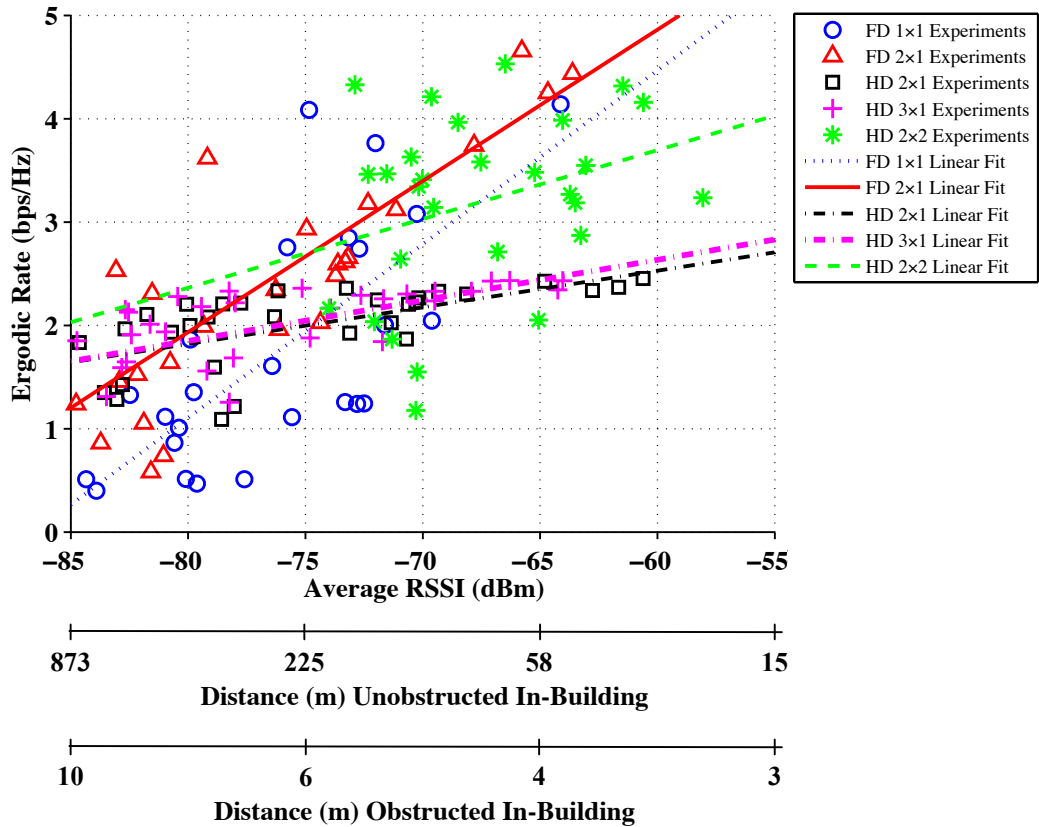


Figure 5.4: Ergodic rate vs. average RSSI for full-duplex and half-duplex systems. Results correspond to experiments performed with nodes using Antenna Placement A2 with a device.

full-duplex and half-duplex systems for a wide range of RSSI values, distances, and LOS/NLOS conditions. Such an extensive characterization is the first of its kind for full-duplex wireless communication systems. We also note that ergodic rate versus RSSI results as shown in Figure 5.4 can be useful for including full-duplex as a mode in Wi-Fi: a device will chose to operate in full-duplex mode for RSSIs where full-duplex achieves larger rates than half-duplex.

## 5.4 Importance of Per-Subcarrier Cancellation

We have demonstrated that antenna placement around a device contributes to the total self-interference cancellation and performance improvement of full-duplex

systems. In this section we show that when interfering antennas are placed around a device, the self-interference channel is not frequency flat and for this scenario the best analog cancellation is achieved when the analog cancellation signal can be adjusted per subcarrier, as required due to the self-interference channel frequency response. In the process, we also demonstrate that if the cancellation signal cannot be adjusted per subcarrier, as is the case for the analog canceller implementations in [3–5], the system performance degrades when the self-interference channel is not frequency flat.

#### 5.4.1 Analysis of the Cancellation Coefficient Required Per Subcarrier

In our implementation of the analog canceller we compute the cancellation coefficient per subcarrier,  $b_{i,m,n}[k]$ , as shown in Equation (2.5). Hence,  $b_{i,m,n}[k]$  is the ratio of the estimate of the self-interference wireless channel  $\hat{h}_{i,m,n}[k]$  and the wire channel  $\hat{h}_{i,n}^W[k]$ . Since the wire channel  $\hat{h}_{i,n}^W[k]$  is frequency flat, variations of the cancellation coefficient  $b_{i,m,n}[k]$  as a function of the subcarrier index will be due to variations of the self-interference channel  $\mathbf{h}_{i,m,n}$  as a function of frequency. If  $\mathbf{h}_{i,m,n}$  is frequency flat then  $b_{i,m,n}[k]$  will be the same across all subcarriers. If  $\mathbf{h}_{i,m,n}$  is frequency selective then  $b_{i,m,n}[k]$  will vary for different subcarriers.

Figure 5.5 shows the magnitude of the cancellation coefficient,  $|b_{i,m,n}[k]|$ , for each used subcarrier for two different packets in our experiments. The subcarrier spacing is 0.3125 MHz as in Wi-Fi for a 20 MHz bandwidth channel. We observe that as a function of subcarriers, the channel attenuation can vary significantly across frequency, and thus approximating the self-interference channel as frequency flat can be highly inaccurate.

To completely characterize the statistical variations in self-interference channel across frequency, we use the measure of peak-to-peak (p2p) value of the magnitude

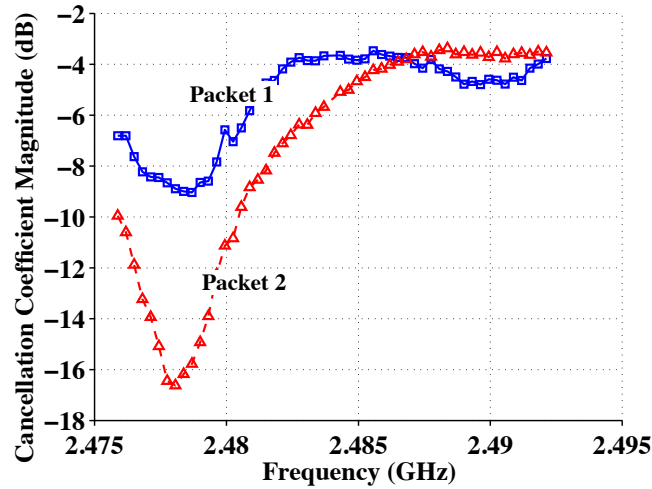


Figure 5.5: Cancellation coefficient per subcarrier captured for two subsequent packets.

of the cancellation coefficient,  $|b_{i,m,n}|^{p2p}$ , as follows,

$$|b_{i,m,n}|^{p2p} = \frac{\max_{k \in \{1, \dots, K\}} |b_{i,m,n}[k]|^2}{\min_{k \in \{1, \dots, K\}} |b_{i,m,n}[k]|^2}. \quad (5.9)$$

If the self-interference channel  $\mathbf{h}_{i,m,n}$  is a flat frequency channel then  $|b_{i,m,n}|^{p2p} = 1$  and for a frequency selective channel  $|b_{i,m,n}|^{p2p}$  will be larger than 1. For each FD  $2 \times 1$  packet we computed the value of  $|b_{i,m,n}|^{p2p}$  between transmitter antenna 1 (T1) and receiver antenna 1 (R1). Figure 5.6 shows a characterization of the magnitude of the cancellation coefficient for the four different configurations listed in Table 3.3. Figure 5.6 shows that the channel can have large variations in magnitude in the practical case of antennas placed around a device (9 dB on average for A2 with device).

Comparing Figure 5.6 with Figure 4.1, we observe the following. The larger the passive suppression, the larger the variations of the self-interference channel as a function of frequency. Intuitively this makes sense since passive suppression of the self-interference corresponds to suppression of the strongest paths between self-interfering antennas. Consequently, the self-interference channel becomes more dependent on

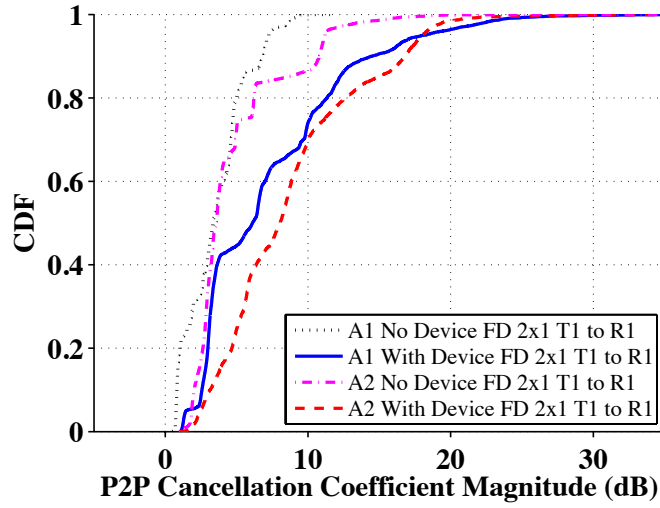


Figure 5.6: CDF of the peak-to-peak value of the cancellation coefficient magnitude.

weaker reflected multi paths and this results in larger frequency selectivity of the self-interference channel.

For scenarios where the channel is frequency-selective, the active analog cancellation must be able to adapt to the frequency variations of the channel per subcarrier, as is the case in our proposed implementation of active analog cancellation.

#### 5.4.2 Effects of Analog Cancellation and Frequency Selectivity on Ergodic Rates

To better illustrate the importance of the per subcarrier adaptation of the analog canceller, we compare the performance of our per subcarrier analog cancellation with the performance of two analog cancellation schemes that do not adapt the magnitude of the cancellation coefficient per subcarrier and use the same magnitude of the cancellation coefficient for all subcarriers (as is the case for the analog canceller schemes considered in [3–5]).

Specifically, we consider the following two flat-frequency cancellers. (i) Flat-Frequency Canceller 1 (FFC1): for this canceller the magnitude of the cancella-

tion coefficient is the same for all subcarriers and is computed as the average from the required per subcarrier as  $(1/K) \sum_{k=1}^K |b_{i,m,n}[k]|$ . (ii) Flat-Frequency Canceller 2 (FFC2): for this canceller the magnitude of the cancellation coefficient is the same for all subcarriers and is computed as the value required by the middle subcarrier in the band hence it is equal to  $|b_{i,m,n}[K/2]|$ . We highlight that the three active cancellers we will compare are different in the magnitude of the cancellation coefficient but apply the same phase of the cancellation coefficient per subcarrier. This simplified implementation for comparison while still allowing us to demonstrate the importance of per subcarrier adaptation.

Figure 5.7 shows the amount of active analog cancellation that our proposed analog cancellation achieves for configuration A2 with device and it also shows the performance of FFC1 and FFC2. We observe that per subcarrier adaptation of the magnitude of the cancellation coefficient achieves larger cancellation values than FFC1 and FFC2. The lower active analog cancellation achieved by FFC1 and FFC2 in a frequency selective environment results in a degradation of the ergodic rate performance as shown in Figure 5.8. More specifically, we observe from results in Figure 5.8 that at an average RSSI of  $-70$  dBm, schemes FFC1 and FFC2 result in an 11% performance loss compared to our proposed scheme.

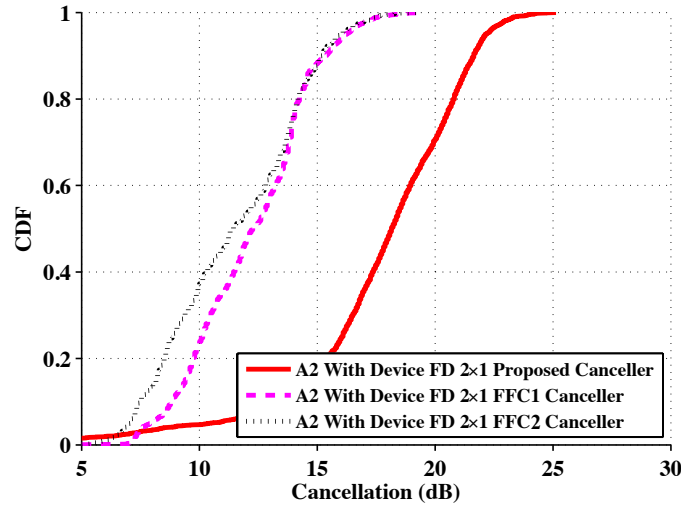


Figure 5.7: CDF of the analog cancellation for different analog cancellers

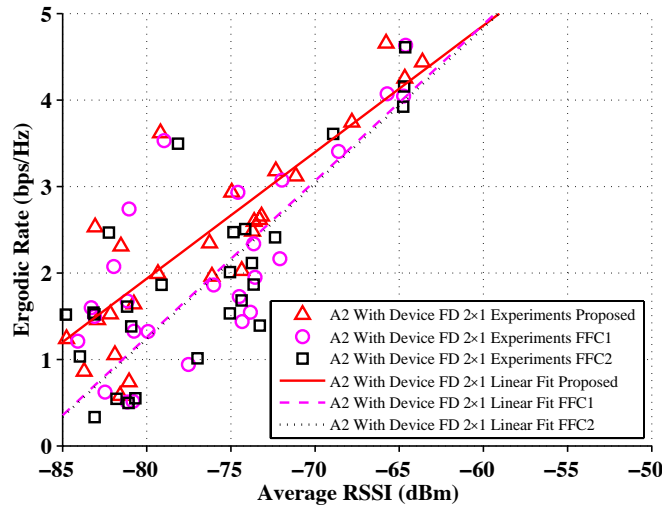


Figure 5.8: Ergodic rate vs. Average RSSI performance for different analog cancellers

## 6.1 Significance and Implications

This thesis presents the first design for a full-duplex multi antenna 20 MHz Wi-Fi-ready system. We have achieved the best self-interference cancellation reported so far. Our design achieves high rate and extended range, adequate for satisfying most indoor Wi-Fi deployments.

Our characterization of passive suppression and active cancellation is the most extensive and complete to date. All previous work has only reported average cancellation values. In this thesis we have presented the following. (a) A statistical, CDF based characterization, of the amount of cancellation achieved by passive suppression and active cancellation. (b) A characterization of the amount of active self-interference cancellation as a function of the self-interference power which shows that the amount of active cancellation increases as the self-interference before active cancellation increases. (c) An analysis of the performance of digital cancellation after analog cancellation which demonstrates that concatenation of analog and digital cancellation does not result in a sum of their individual cancellations measured in isolation.

Our complete characterization of the self-interference cancellation together with our ergodic rate analysis allows us to be the first to explain and demonstrate that if both communicating devices in a full-duplex two-way link increase their transmission power, then the total ergodic sum rate of the system increases.

Our results illustrated the factors that dominate the performance of full-duplex wireless communications and lead to new design rules for the implementation of these systems. Further, we believe that our results conclusively show that full-duplex Wi-Fi is possible and can be highly beneficial in practical configuration environments.

## 6.2 Future Directions

In this thesis we have focused our attention on the analysis of full-duplex two-way communications. Another application of full-duplex communications is in the area of full-duplex relays. Theoretical work has been done in this area by authors in [21–23]. Recent experiment based analysis has been reported in [24]. Our analysis of the self-interference cancellation is valid either in a two-way full-duplex configuration or a full-duplex relay configuration.

We have demonstrated the feasibility and the gains of full-duplex on a physical layer level. The next step to enable rapid adoption of full-duplex wireless is the design of novel Medium Access Control (MAC) protocols that can leverage the full-duplex gains that we have demonstrated. Recent work on this area has been presented in [7, 25, 26], however, the design and evaluation of protocols for full-duplex is still at an early stage.

## BIBLIOGRAPHY

---

- [1] S. Chen, M. Beach, and J. McGeehan, “Division-free duplex for wireless applications,” In *IEEE Electronics Letters*, **34**, 147–148 (1998).
- [2] D. W. Bliss, P. Parker, and A. R. Margetts, “Simultaneous Transmission and Reception for Improved Wireless Network Performance,” In *IEEE/SP 14th Workshop on Statistical Signal Processing*, pp. 478–482 (2007).
- [3] B. Radunovic, D. Gunawardena, P. Key, A. P. N. Singh, V. Balan, and G. Dejean, “Rethinking Indoor Wireless: Low power, Low Frequency, Full-duplex,” Technical report, Microsoft Research (2009) .
- [4] J. I. Choi, M. Jain, K. Srinivasan, P. Levis, and S. Katti, “Achieving single channel, full duplex wireless communication,” In *Proceedings of ACM Mobicom*, pp. 1–12 (2010).
- [5] M. Jain, J. Choi, T. M. Kim, D. Bharadia, S. Seth, K. Srinivasan, P. Levis, S. Katti, and P. Sinha, “Practical, real-time full duplex wireless,” In *Proceedings of ACM Mobicom*, pp. 301–312 (2011).
- [6] M. A. Khojastepour, K. Sundaresan, S. Rangarajan, X. Zhang, and S. Barghi, “The case for antenna cancellation for scalable full-duplex wireless communications,” In *Proceedings of Hotnets*, pp. 1–17 (2011).
- [7] A. Sahai and G. Patel and A. Sabharwal, “Pushing the limits of Full-duplex: Design and Real-time implementation,” In *arXiv.org:1107.0607*, (2011).

- 
- [8] A. Sahai, G. Patel, and A. Sabharwal, “Asynchronous Full-duplex Wireless,” In *Proceedings of COMSNETS*, pp. 1–9 (2012).
- [9] T. Rappaport, *Wireless Communications: Principles and Practice*, 2nd ed. (Prentice Hall, Upper Saddle River, NJ, USA, 2001).
- [10] A. Raghavan, E. Gebara, E. M. Tentzeris, and J. Laskar, “Analysis and design of an interference canceller for collocated radios,” *IEEE Transactions on Microwave Theory and Techniques* **53**, 3498–3508 (2005).
- [11] “QHX220 Active Isolation Enhancer and Interference Canceller.” [Online]. Available: <http://www.intersil.com/data/fn/fn6986.pdf>.
- [12] “RE07U-SM Antenna.” [Online]. Available: <http://www.l-com.com/item.aspx?id=21447>.
- [13] “SMA Female Power Divider.” [Online]. Available: <http://www.pasternack.com/Pdf/PE2014.pdf>.
- [14] S. M. Alamouti, “A Simple Transmit Diversity Technique for Wireless Communications,” *IEEE Journal on Selected Areas in Communications* **16**, 1451–1458 (1998).
- [15] “MATLAB Communications System Toolbox R2011b.” [Online]. Available: [www.mathworks.com](http://www.mathworks.com).
- [16] “WARPLab Framework.” [Online]. Available: <http://warp.rice.edu/trac/wiki/WARPLab>.
- [17] “WARP Repository.” [Online]. Available: <http://warp.rice.edu/trac/wiki/PapersandPresentations>.

- 
- [18] M. Duarte, C. Dick, and A. Sabharwal, “Experiment-driven Characterization of Full-Duplex Wireless Systems,” Submitted to IEEE Transactions on Wireless Communications (2011).
- [19] D. Tse and P. Viswanath, *Fundamentals of Wireless Communications* (Cambridge University Press, New York, NY, USA, 2005).
- [20] M. Duarte, A. Sabharwal, C. Dick, and R. Rao, “Beamforming in MISO Systems: Empirical Results and EVM-based Analysis,” IEEE Transactions on Wireless Communications **9**, 3214–1276 (2010).
- [21] T. Riihonen, S. Werner, and R. Wichman, “Optimized gain control for single-frequency relaying with loop interference,” IEEE Transactions on Wireless Communications **8**, 2801–2806 (2009).
- [22] T. Riihonen, S. Werner, and R. Wichman, “Hybrid Full-Duplex/Half-Duplex Relaying with Transmit Power Adaptation,” IEEE Transactions on Wireless Communications **10**, 3074–3085 (2011).
- [23] T. Riihonen, S. Werner, and R. Wichman, “Mitigation of Loopback Self-Interference in Full-Duplex MIMO Relays,” IEEE Transactions on Wireless Communications **59**, 5983–5993 (2011).
- [24] E. Everett, M. Duarte, C. Dick, and A. Sabharwal, “Empowering Full-Duplex Wireless Communication by Exploiting Directional Diversity,” In *Asilomar Conference on Signals, Systems, and Computers*, (2011).
- [25] S. Sen, R. R. Choudhury, and S. Nelakuditi, “CSMA/CN: Carrier Sense Multiple Access with Collision Notification,” In *Proceedings of ACM Mobicom*, (2010).
- [26] N. Singh and D. Gunawardena and A. Proutiere and B. Radunovic and H. V. Balan and P. Key, *Proceedings of WiOpt* (2011).